Journal of Medicinal Chemistry

pubs.acs.org/jmc Article

Sialyltransferase Inhibitors Suppress Breast Cancer Metastasis

Chih-Wei Fu, Han-En Tsai, Wei-Sheng Chen, Tzu-Ting Chang, Chia-Ling Chen, Pei-Wen Hsiao, and Wen-Shan Li*

Cite This: J. Med. Chem. 2021, 64, 527−542 Read Online

ACCESS | Metrics & More | Article Recommendations | Supporting Information

ABSTRACT: We report the synthesis and evaluation of a series of cell-permeable and N- versus O-selective sialyltransferase inhibitors. Inhibitor design entailed the functionalization of lithocholic acid at C(3) and at the cyclopentane ring side chain. Among the series, FCW34 and FCW66 were shown to inhibit MDA-MB-231 cell migration as effectively as ST3GALIII-gene knockdown did. FCW34 was shown to inhibit tumor growth, reduce angiogenesis, and delay cancer cell metastasis in animal models. Furthermore, FCW34 inhibited vessel development and suppressed angiogenic activity in transgenic zebrafish models. Our results provide clear evidence that FCW34-induced sialyltransferase inhibition reduces cancer cell metastasis by decreasing N-glycan sialylation, thus altering the regulation of talin/integrin/FAK/paxillin and integrin/NFκB signaling pathways.

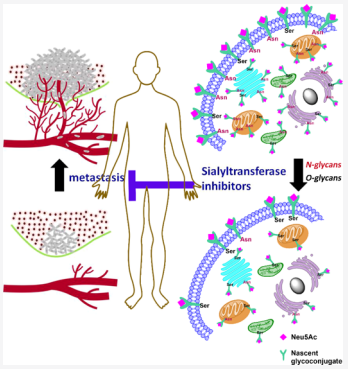

INTRODUCTION

Metastasis is the primary cause of death in cancer patients. The multistep process by which cancer cells migrate from the tumor site to reach and proliferate in secondary organs is known as the metastatic cascade. During this process, cancer cells detach from the tumor, move through basement membrane barriers and the extracellular matrix (ECM), enter the vascular system, and adhere to a new site where they proliferate.[1−3] Inhibitors that can block this process are urgently needed.

The known correlation between metastasis and abnormally high levels of N- and O-sialylation of cancer-cell surface glycoproteins[4−8] directed our attention to the development of chemical compounds to inhibit glycoprotein sialylation, which is catalyzed by members of the sialyltransferase (ST) family.[9] The ST family comprises more than 20 glycoprotein-specific and glycolipid-specific, α2,3-, α2,6-, and α2,8-linkage transferring enzymes.[10,11] The ST family is known to play an important role in tumor cell progression, invasion and metastasis,[12−15] especially in breast cancer.[16−18] Previous studies have shown that overexpression of genes encoding the sialyltransferases ST6GALI and ST3GALIV protects tumor cells against hypoxia, modulates tumor progression, adhesion and migration in pancreatic cancer cell lines, and enhances the metastatic potential of cancer cells in vivo.[19−23] Furthermore, the sialyltransferase ST6GALNACV is known to mediate breast cancer metastasis to the brain.[24]

Despite ample documentation of the importance of post-translational sialylation of glycoproteins and glycolipids to the regulation of immune cells[25] or cell−cell adhesion and to the regulation of tumor cell metastasis and invasion, an inhibitor with ST isozyme preference has yet to be identified for application in in vitro studies or for in vivo use to repress cancer metastasis. With few exceptions,[26−29] inhibitor designs have concentrated on creating tight-binding substrate analogues.[30−39] Because most of these inhibitors are not cell permeable, their use in biological and clinical applications is restricted. To overcome the availability of STs, recent advances in the design of various expression systems for recombinant enzyme production open up the opportunity to screen compounds against a wider panel of ST enzymes.[40] In addition, inhibitors that can preferentially act on ST isozymes have not yet been reported. Thus, the discovery of cell-permeable inhibitors that can target specific ST isozymes in vivo, and thus, minimize potential side effects, is essential for the development of effective chemical therapeutics to prevent metastasis.

RESULTS AND DISCUSSION

Design of Isozyme-Specific and Cell-Permeable ST Inhibitors by Employing the "LCA-Extension Strategy". In an earlier work, we discovered that the lithocholic acid (LCA)[41] component of the natural product soyasaponin I serves as an ideal platform for the development of cell-permeable ST inhibitors.[42−44] Specifically, the LCA adducts Lith-*O*-Asp and AL10 depicted in Figure 1 were shown to

Received: August 24, 2020
Published: December 28, 2020

https://dx.doi.org/10.1021/acs.jmedchem.0c01477
J. Med. Chem. 2021, 64, 527−542

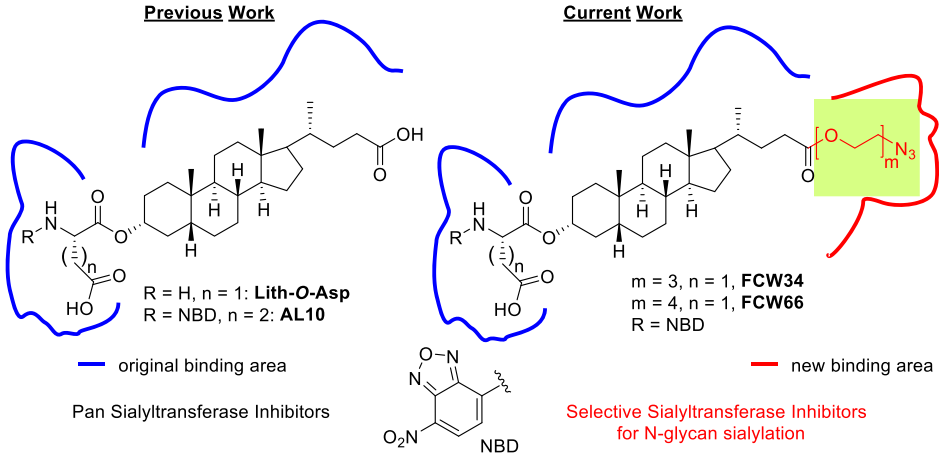

Figure 1. Illustration of the lead ST inhibitors discovered in previous work (left panel) and two second-generation inhibitors examined in the current work. The blue line defines the lead-inhibitor-binding site of the ST, whereas the red line depicts a hypothetical subsite to be filled by the PEG moiety of the second-generation inhibitors. NBD is the abbreviation for nitrobenzoxadiazole.

Table 1. Inhibitory Potency and Specificity of Sialyltransferase Inhibitors

Cpd	IC_{50} (μM)			selectivity ratio	
	α2,3-*N*-ST3GALIII[g]	α2,6-*N*-ST6GALI[g]	α2,3-*O*-ST3GALI[g]	α2,3-*O*-/α2,3-*N*-	α2,3-*O*-/α2,6-*N*-
2aA	0.8 ± 0.1	4.2 ± 0.3	0%[a]	>625[d]	>119
2bA	0.77 ± 0.02	4.33 ± 0.04	0%[a] (74%)[b]	>649[d] (<1299)[e]	>116
2cA (FCW34)	1.74 ± 0.09	3.6 ± 0.4	0%[a] (60%)[b]	>287[d] (<575)[e]	>139
2dA (FCW66)	1.01 ± 0.07	4.90 ± 0.08	0%[a] (50%)[b]	>495[d] (≤990)[e]	>102
2eA	1.0 ± 0.1	5.0 ± 0.2	0%[a]	>516[d]	>99
3aB	[c]	7.2 ± 0.1	0%[a]	[c]	>70
3bB	[c]	6.7 ± 0.3	0%[a]	[c]	>74
3cB	[c]	5.4 ± 0.5	0%[a]	[c]	>94
3dB	[c]	5.7 ± 0.4	0%[a]	[c]	>88
3eB	[c]	7.5 ± 0.4	0%[a]	[c]	>67
4aC	[c]	5.6 ± 0.2	0%[a]	[c]	>89
4bC	[c]	5.1 ± 0.1	0%[a]	[c]	>97
4cC	[c]	4.6 ± 0.4	0%[a]	[c]	>109
4dC	[c]	5.0 ± 0.4	0%[a]	[c]	>101
4eC	[c]	5.7 ± 0.4	0%[a]	[c]	>88
Lith-*O*-Asp	12	15.8 ± 0.1	39 ± 1	3	3
AL10	0.9 ± 0.1	1.5 ± 0.5	13.2 ± 0.6	15	9
LCAG	[c]	0%[f]	15%[a] (41%)[b]		
Soyasaponin I	[c]	68%[f]	59%[a] (83%)[b]		

[a]Inhibition percentage was measured at 500 μM. [b]Inhibition percentage was measured at 1 mM. [c]Not determined. [d]The selectivity ratio, in parentheses, is expressed as the value of 500 μM/individual IC_{50} from α2,3-*N*-ST3GALIII without correction for the contribution of IC_{50} from α2,3-*O*-ST3GALI. [e]The selectivity ratio, in parentheses, is expressed as the value of 1000 μM/individual IC_{50} from α2,3-*N*-ST3GALIII without correction for the contribution of IC_{50} from α2,3-*O*-ST3GALI. [f]Inhibition percentage was measured at 100 μM. [g]The selected ST isozymes, rat α2,3-*N*-ST3GALIII (CalBiochem #566218), human α2,6-*N*-ST6GALI (R&D systems #7620-GT), and rat α2,3-*O*-ST3GALI (CalBiochem #566227), were used in this study.

exhibit low micromolar inhibitory activity against several sialyltransferases, ST3GALIII, ST6GALI, and ST3GALI (Table 1; the IC_{50} range is 12−39 and 0.9−13.2 μM, respectively), as well as to display significant antimetastatic properties.[42−44] To increase the affinity for a target protein, chemically designed compounds will be used to probe biologically relevant chemical space and improve the potency against different isoforms of enzymes based on a structure-based design approach. From structural minimization and visualization of AL10 and the designed ST inhibitors, we observed an extended space with hydrophobic and hydrophilic amino acid residues, such as P320(B), P259(B), V261(A), W302(B), H370(B), S322(B), S189(B), C353(B), G324(B), A190(B), and N212(B) in two asymmetric polypeptide chains (A/B) of ST6GALI (PDB 6QVT), where the polyethylene glycol (PEG) moiety of designed inhibitors might develop additional interactions (see the Molecular Docking section and Supporting Information). In the present study, the lead inhibitor Lith-*O*-Asp was modified to extend the cyclopentane ring side chain with one or more ethylene glycol units and elaborate the C(3) aspartate ester moiety, as is illustrated in Figure 1 with the Lith-*O*-Asp analogues FCW34 and FCW66. By employing this "LCA-extension strategy", we set out to generate isozyme-specific, cell-permeable ST inhibitors. The three series of compounds prepared are shown in Scheme 1. The "**2A**" series, which includes FCW34 and FCW66,

https://dx.doi.org/10.1021/acs.jmedchem.0c01477
J. Med. Chem. 2021, 64, 527−542

Scheme 1. Synthesis of ST Inhibitors[a]

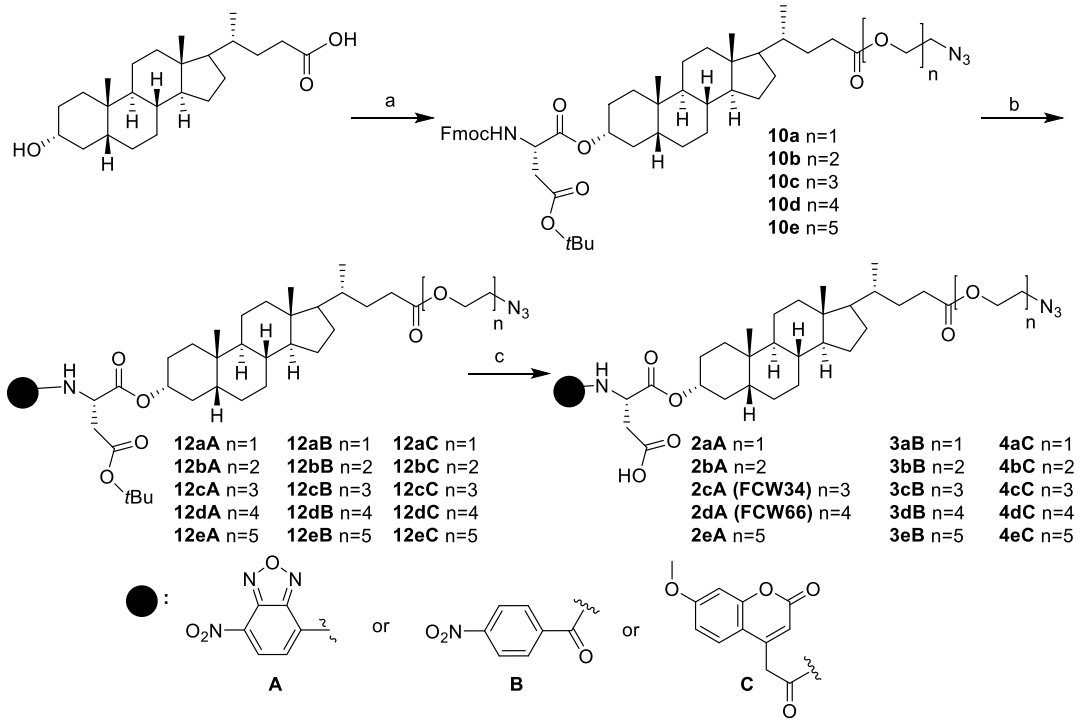

[a]Reagents and conditions: (a) (i) Fmoc-L-Asp(O-*t*Bu)-OH, DCC, DMAP, CH_2Cl_2, RT, 8 h, 50%; (ii) **1a**−**1e** N_3 linker, DCC, DMAP, CH_2Cl_2, RT, 3 h, (**10a** 88%, **10b** 86%, **10c** 80%, **10d** 71%, **10e** 75%); (b) (i) DBU, CH_2Cl_2, RT, 2 h; (ii) NBD-Cl, $NaHCO_3$, THF-EtOH, RT, 2 d or *p*-nitrobenzoic acid, 2-(7-methoxy-2-oxo-2*H*-chromen-4-yl)acetic acid, HBTU, DIPEA, CH_2Cl_2, RT, 3 h (two steps: **12aA** 45%, **12bA** 32%, **12cA** 34%, **12dA** 31%, **12eA** 32%, **12aB** 91%, **12bB** 87%, **12cB** 72%, **12dB** 73%, **12eB** 70%, **12aC** 88%, **12bC** 83%, **12cC** 75%, **12dC** 75%, **12eC** 68%); (c) TFA, H_2O, CH_2Cl_2, RT, 2 h (**2aA** 85%, **2bA** 82%, **2cA**(**FCW34**) 91%, **2dA**(**FCW66**) 88%, **2eA** 85%, **3aB** 80%, **3bB** 82%, **3cB** 90%, **3dB** 82%, **3eB** 84%, **4aC** 90%, **4bC** 82%, **4cC** 85%, **4dC** 80%, **4eC** 82%).

possesses the C(3) *N*-nitrobenzoxadiazole (NBD)-L-aspartate ester moiety, whereas the "**3B**" series possesses a *N*-*p*-nitrophenyl (NP)-L-aspartate ester moiety, and the "**4C**" series a *N*-7-methoxycoumarin (MC)-L-aspartate ester moiety. Within each of the three series, the annotations **a**−**d** correspond to the number of ethylene glycol (EC) units that make up the PEG moiety. These three moieties, NBD, NP, and MC, were uncovered through the initial screening of SAR study using the drug-like substructure. The inclusion of NBD moiety is based on the substructure of benzoxadiazole group from Isradipine, approved by the FDA for medical use in 1989.

Synthesis of ST Inhibitors. Steps taken toward the chemical synthesis of **2aA**−**2eA**, **3aB**−**3eB**, and **4aC**−**4eC** are summarized in Schemes 1, S1 and S2 (for chemical structures: see Supporting Information Chart S1). Synthetic intermediates **10a**−**10e** were prepared via dicyclohexylcarbodiimide (DCC)-promoted esterification of LCA with Fmoc-Asp(*t*-Bu)-OH and with PEG-N_3 linkers of varying lengths (**1a**−**1e**, see the Supporting Information). Removal of the Fmoc-protecting group from **10a**−**10e** with 1,8-diazabicyclo[5.4.0]undec-7-ene (DBU) to generate the free amine was followed by amination with NBD-Cl under basic conditions to yield **12aA**−**12eA**, or by amide coupling with *p*-nitrobenzoic acid or 2-(7-methoxy-2-oxo-2*H*-chromen-4-yl)acetic acid, using HBTU as the coupling reagent, to furnish **12aB**−**12eB** or **12aC**−**12eC**. Removal of the *t*-Bu-protecting group with TFA provided the final products **2aA**−**2eA**, **3aB**−**3eB**, and **4aC**−**4eC**.

Activity and Isozyme Selectivity of ST Inhibitors In Vitro. The inhibition of selected ST isozymes rat α2,3-*N*-ST3GALIII, human α2,6-*N*-ST6GALI, and rat α2,3-*O*-ST3GALI with compounds Lith-*O*-Asp, **2aA**−**2eA**, **3aB**−**3eB**, and **4aC**−**4eC** was monitored using the UPLC-based inhibition assay. The IC_{50} values determined for the tight-binding ST isozyme−inhibitor pairs and the % inhibition determined for the weak-binding ST isozyme−inhibitor pairs are reported in Table 1 (lithocholylglycine, LCAG, and soyasaponin I as the positive control). The series **2aA**−**2eA** displayed an order of magnitude tighter binding to α2,3-*N*-ST3GALIII (IC_{50} range is 0.8−1.7 μM) compared to Lith-*O*-Asp (IC_{50} = 12 μM). In contrast, while the IC_{50} value determined for Lith-*O*-Asp inhibition of α2,3-*O*-ST3GALI is 39 μM, the IC_{50} values measured for **2aA**−**2dA** are ∼1 mM and for **2eA** IC_{50} > 1 mM. Likewise, whereas **2aA**−**2eA**, **3aB**−**3eB**, and **4aC**−**2eC** display ∼2−3-fold tighter binding to α2,6-*N*-ST6GALI (IC_{50} values: 4−7 μM) than that observed with Lith-*O*-Asp (IC_{50} value: 16 μM), they do not show inhibition of α2,3-*O*-ST3GALI when tested at a concentration of 1 mM, in contrast to IC_{50} = 39 μM measured for Lith-*O*-Asp. These results indicate that **2aA**−**2eA**, **3aB**−**3eB**, and **4aC**−**2eC** can be used to inhibit the two *N*-glycoprotein sialyltransferases α2,3-*N*-ST3GALIII and α2,6-*N*-ST6GALI without impacting the activity of the *O*-glycoprotein sialyltransferase α2,3-*O*-ST3GALI.

The design ideas were inspired by the results of previous inhibitory potency studies of LCA and its analogues toward ST isozymes.[10] Further employing the "LCA-extension strategy leads to the discovery of target compounds, FCW34 and FCW66. The complete structure−activity relationship and optimization are depicted in Figure S1. Our initial studies focused on the effect of C(3) amino acid moiety and observed

https://dx.doi.org/10.1021/acs.jmedchem.0c01477
J. Med. Chem. 2021, 64, 527−542

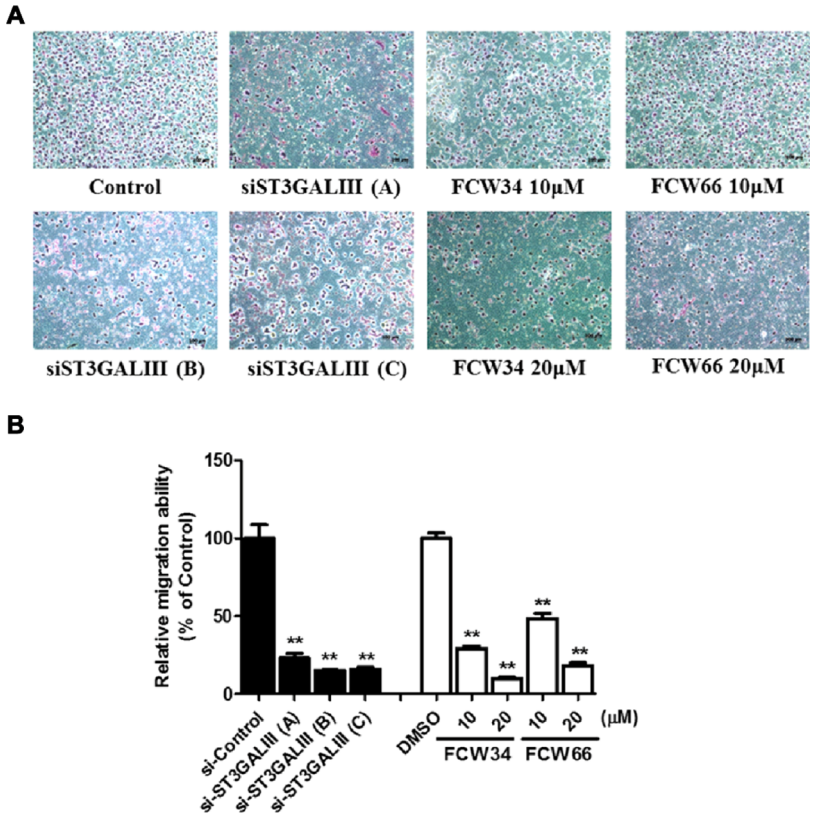

Figure 2. A comparison of the effects of siRNA-induced ST3GALIII gene knockdown with those of FCW34- and FCW66-induced ST3GALIII inhibition on the migration ability of MDA-MB-231 cells in vitro. (A) Images of cells transfected with three ST3GALII siRNA A, B, and C (STEALTH siRNAs, HSS143938, HSS143939, and HSS143940 from Thermo Fisher with different target sequences), respectively, for 72 h or exposed to 10 or 20 μM FCW34 or FCW66 and allowed to migrate for 16 h (see the Supporting Information). (B) A plot of results from (A) in the chart format. All data were expressed as mean ± SEM of three experiments (*P < 0.05, **P < 0.01).

LCA with a specific amino acid sequence, such as L-Asp-LCA, L-Glu-LCA, D-Glu-LCA, L-Asp-L-Asp-LCA, and L-Asp-L-Asp-Gly-Gly-LCA, displaying potent inhibitory activity against human STs, α2,3-*N*-ST, and α2,6-*N*-ST, respectively.[28,29] Building on the optimal structure of L-Asp-LCA, we extended the additional groups in the N-terminal of Asp and found the heterocyclic moiety (NBD, NP, and MC) exhibiting greater inhibitory activities against α2,3-*N*-ST, α2,3-*O*-ST, and α2,6-*N*-ST compared to that of L-Asp-LCA (Lith-*O*-Asp), suggesting that perhaps a heterocyclic moiety at the N-terminal position could occupy an interactive region in the active site pocket of ST isozyme. For example, AL10, possessing an NBD group at the N-terminal position, displayed improved inhibitory potency against α2,3-*N*-ST, α2,3-*O*-ST, and α2,6-*N*-ST with respective IC_{50} values of 0.9, 13.2, and 1.5 μM (Table 1), which are with 3−13-fold increased potency over L-Asp-LCA (Lith-*O*-Asp). Besides redesigning the potent ST inhibitors based on previous results, the approach to solely tune the steroidal core structure (Figure S1), the B- and C-ring-modified homolactones and homolactams,[26] was accomplished to uncover several improved ST inhibitors, as compared to the parent compound LCA, indicating that the modified homolactones and homolactams are located inside the binding pocket and the B- and C-rings are proximal to the hydrophilic region in the active site of the ST isozyme. As we knew, the structure of LCA belongs to the "tadpole scaffold" and relatively few positions are available where additional substituents can be added. To explore the target-binding site for further binding regions to achieve additional binding interactions, we use the "LCA-extension strategy" to extend the cyclopentane ring side chain with one or more ethylene glycol units (n = 1−5). This action leads to the discovery of ST inhibitors with isozyme preference, FCW34 and FCW66 (Figure 1 and Table 1). According to the SAR results in (Figure S1), the cyclopentane ring side chain with one or more ethylene glycol units play an important role in ST isozyme selectivity. Perhaps the extension of the cyclopentane ring side chain is allowed in the active sites of α2,3-*N*-ST and α2,6-*N*-ST; however, this action cannot be accommodated by α2,3-*O*-ST.

ST Inhibitors Inhibit the Migration Ability of Breast Cancer Cells via Suppression of α2,3-*N*-ST3GALIII-Catalyzed *N*-Glycoprotein Sialylation. The patients of triple-negative breast cancer (TNBC) respond poorly to the treatment of both endocrine therapy and HER2-targeted therapy. The treatments available against TNBC are mainly surgery, radiation, and chemotherapy in clinic practice. To overcome the limited treatment options, we plan to accelerate the development of an innovative ST inhibitor to gain new targeted therapies for TNBC patients. The MDA-MB-231 cell line is used in this study as it represents one of the important cell lines of TNBC. Our next goal was to determine if the second-generation ST inhibitors **2aA**−**2eA** also inhibit breast cancer cell motility. Before that, the antiproliferative effect of compounds **2aA**−**2eA**, **3aB**−**3eB**, and **4aC**−**4eC** was tested on MDA-MB-231 cells. All of them did not cause an inhibitory effect on cell growth (>90% survival) at the tested concentrations (>60 μM). For this purpose, the Boyden

https://dx.doi.org/10.1021/acs.jmedchem.0c01477
J. Med. Chem. 2021, 64, 527−542

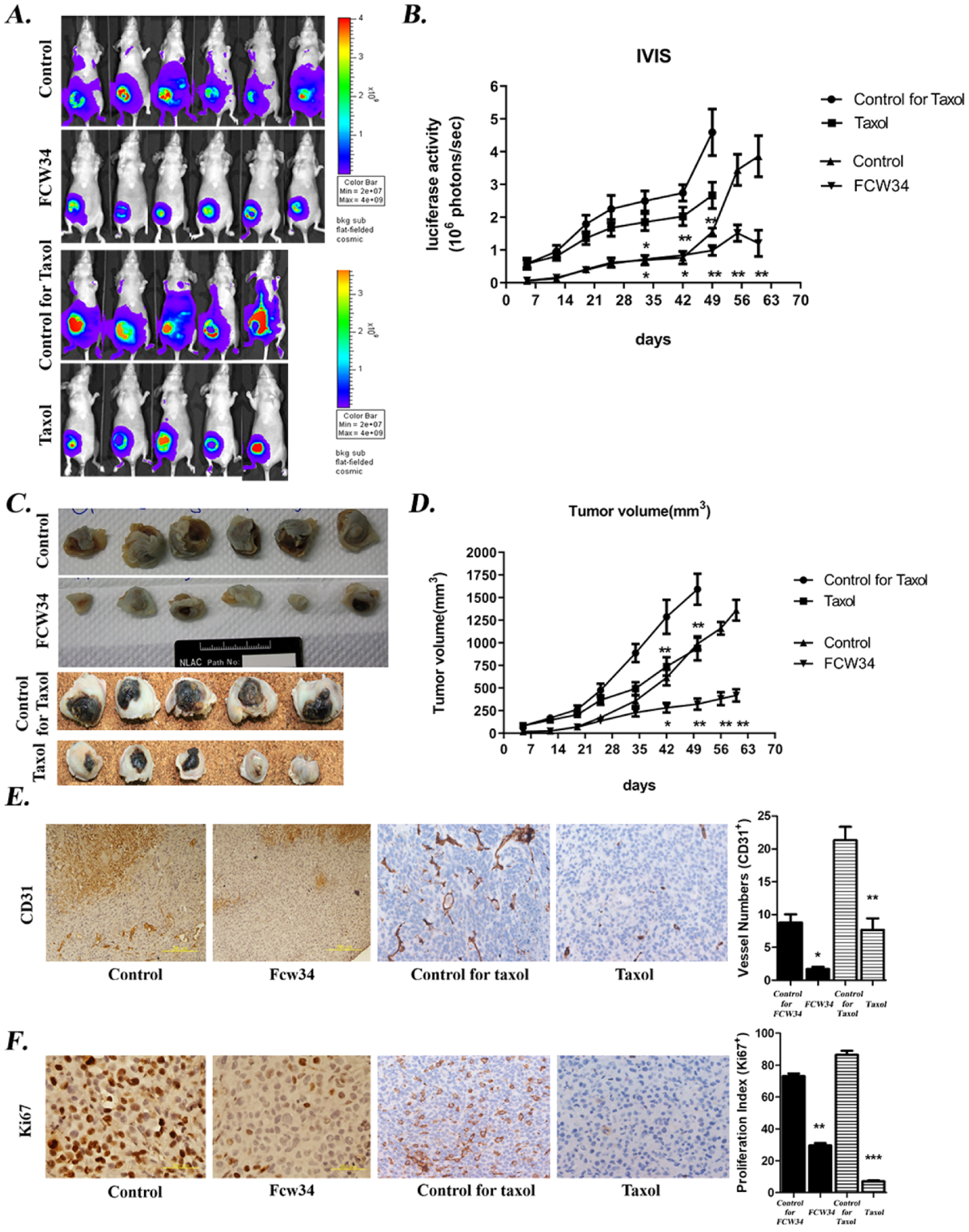

Figure 3. Effects of FCW34 and positive control, Taxol, on tumor progression and angiogenesis of MDA-MB-231 cells in vivo. Mice bearing the established MDA-MB-231/Luc tumors (100 mm^3) were treated with FCW34 (10 mg/kg/mouse/3 d) or Taxol (10 mg/kg/mouse/3 d) as a positive control via intraperitoneal injection. (A) Bioluminescence images taken after 8 weeks and (B) graph showing a comparison of the quantification of photo units between the mice treated with FCW34 after 60 d versus the mice treated with Taxol after 50 d (n = 6 per group). (C,D) After the tumors had reached the size of ~100 mm^3, the mice were treated with vehicle, FCW34, or Taxol, and subsequently, monitored for tumor growth. After the mice were sacrificed, the tumors were harvested for further analysis and the blood vessel network in breast cancer tissues was examined by CD31 immunostaining analysis (E). The number of vessels in the breast cancer tissue counted using the CAST system and expressed as mean ± SEM (n = 6 per group, right panel). (F) The proliferation activity examined by Ki-67 immunostaining and quantification of proliferation index, Ki-67$^+$ cells, in tumor tissues (n = 6 per group, right panel). The asterisks indicate statistical significance (*p < 0.05, **p < 0.01).

https://dx.doi.org/10.1021/acs.jmedchem.0c01477
J. Med. Chem. 2021, 64, 527−542

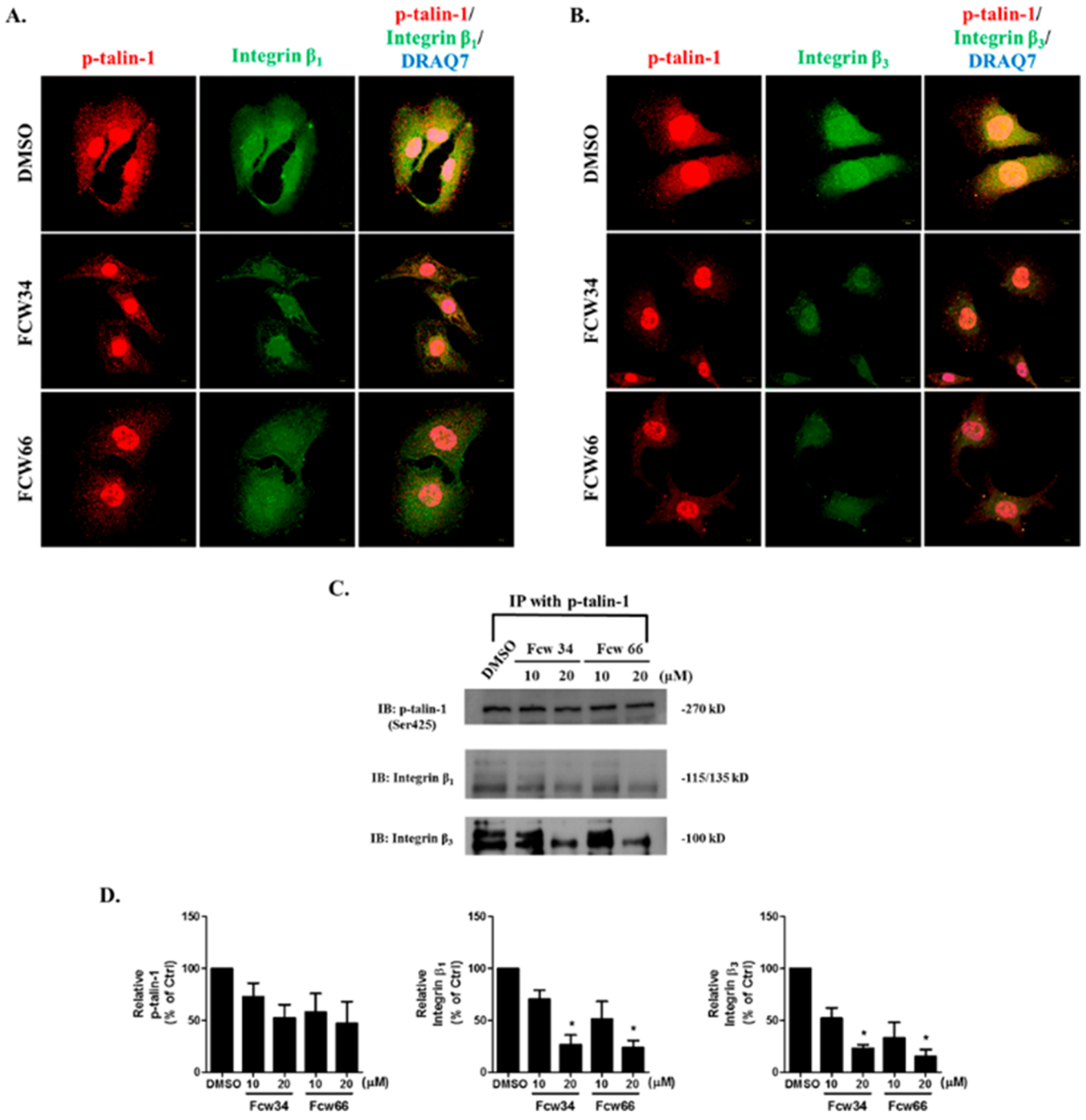

Figure 4. The effects of FCW34 and FCW66 on talin-1 and integrin interaction in cultured MDA-MB-231 cells. (A,B) Colocalization of *p*-talin-1 with integrin β1 or integrin β3 in MDA-MB-231 cells observed by immunofluorescence analysis. After treatment with DMSO (control), 20 μM FCW34, or 20 μM FCW66 for 48 h, the cells were permeabilized with Triton X-100 and stained with anti-*p*-talin-1 (red) and with (A) anti-integrin β1 (green) or with (B) integrin β3 antibodies (green). (C) Western blots of *p*-talin-1 immunoprecipitate from MDA-MB-231 cells treated with DMSO, FCW34, or FCW66 (10 and 20 μM). *p*-Talin-1 and integrins β1 and β3 were detected using the corresponding antibodies. (D) The relative amounts of *p*-talin-1 and integrins β1 and β3 observed in the western blots and reported as mean ± SEM for triplicate experiments.

Chamber assay was used to measure the impact of exposure of MDA-MB-231 cells to (20 μM) inhibitor. Based on the results from this preliminary screen (see Figure S2), **2cA** and **2dA** (hereafter referred to as FCW34 and FCW66, respectively) were identified as having the greatest potency as cancer cell migration inhibitors. To determine the IC_{50} values for FCW34 and FCW66, cell motility was monitored over a 16 h period as a function of their concentration, ranging from 2 to 30 μM. The results obtained (see Figures S3 and S4) demonstrate that both inhibitors abrogate serum-induced cell migration in a concentration-dependent manner and define FCW34 IC_{50} = 10.64 ± 0.09 μM and FCW66 IC_{50} = 12.0 ± 0.1 μM (lithocholylglycine, LCAG, and soyasaponin I as positive control).

To explore a possible link between FCW34 and FCW66 acting as inhibitors of ST3GALIII and cancer cell motility, we

https://dx.doi.org/10.1021/acs.jmedchem.0c01477
J. Med. Chem. 2021, 64, 527−542

examined the effect of α2,3-*N*-ST3GALIII knockdown by α2,3-*N*-ST3GALIII siRNA on cell motility (Figure S5). As shown in Figure 2A,B, compared to the control, knockdown of the α2,3-*N*-ST3GALIII gene significantly inhibited the migration activity in MDA-MB-231 cells, similar to the inhibitory effects observed for FCW34 and FCW66 exposure. Taken together, these findings suggest that FCW34 and FCW66 might retard cancer cell migration via inhibition of α2,3-*N*-ST3GALIII-catalyzed *N*-glycoprotein sialylation.

ST Inhibitors Inhibit the Migration Ability of Breast Cancer Cells via Suppression of Integrin Sialylation. Our next step was to determine if inhibition of integrin sialylation might be the cause of inhibited mobility in cancer cells exposed to FCW34 and FCW66. This possibility was suggested by increasing evidence that protein sialylation plays a critical role in tumor metastasis, coupled with the knowledge that aberrant *N*-glycosylation of integrin, the major cellular receptor of the extracellular matrix in cell migration, is associated with cancer cell behavior.[45−48] Until now, studies designed to elucidate the biological effects of integrin sialylation have been restricted by the limited availability of cell-permeable ST inhibitors. In the present study, western blot analysis of MDA-MB-231 cell extracts was carried out using biotinylated *Maackia amurensis* Lectin II (MAL II) as the probe for (α-2,3)-linked sialic acid residues. We observed that FCW34 and FCW66 significantly suppressed the sialylation of integrin β subunits β1, β3, β4, and β5 (Figure S6).

FCW34 Exhibits In Vivo Spontaneous Metastasis Inhibition and Reduces Tumor Growth. Because Taxol is one of the clinically effective drugs for the treatment of breast cancer, it is used to treat patients with metastatic breast cancer. In order to ensure the accuracy and efficacy of animal experiments, Taxol was selected as the positive control in this experiment. To determine if FCW34 inhibits tumor growth and metastasis in vivo, a BALB/c mice model of MDA-MB-231/Luc was used. As shown in Figure 3A−D, the FCW34- or Taxol-treated mice displayed profound tumor suppression and delayed lung metastasis. The results of histological analysis (Figure S7A) show a significantly smaller number of metastatic foci in the lungs of FCW34- or Taxol-treated mice than in the control mice. In addition, analysis of H&E-stained adjacent lymph node sections revealed fewer metastatic nodules in the FCW34- or Taxol-treated mice than in the control mice (Figure S7B). Finally, the results of blood tests and body weight assessments indicate that treatment of mice with FCW34 or Taxol is not detrimental to their health (Figure S8). Taken together, these findings suggest that FCW34 is an excellent candidate for evaluation as a lead for an antimetastatic drug for cancer treatment.

Having established that FCW34 treatment suppresses tumor growth and metastasis in the mouse model, we carried out further histological analysis of collected tumor tissues to study the molecular mechanisms of FCW34-induced suppression. The cluster of differentiation 31 (CD31) adhesion molecule, also known as platelet-endothelial cell adhesion molecule-1 (PECAM-1), was used as a marker of angiogenesis[49,50] to obtain the immunostaining images shown in Figure 3E. The images reveal a significantly smaller number of vessels surrounding tumor nodules in the FCW34-treated mice than in the control mice. Quantification analysis of vessels confirmed that angiogenesis was significantly reduced in FCW34- or Taxol-treated mice. Next, the extent of tumor proliferation was assessed using the cellular proliferation marker, Ki-67 nuclear protein.[51,52] The synchronized images and the corresponding proliferation indexes shown in Figure 3F reveal that the accumulation of Ki-67-positive cells in the FCW34- or Taxol-treated mice is significantly less than that observed for the control mice. These results indicate that FCW34 inhibits proliferation and neovascularization, and thus, tumor progression.

FCW34 and FCW66 Suppress Cancer Metastasis through Disruption of Talin-Driven Integrin Activation by Reducing *N*-Glycan Sialylation and Talin Phosphorylation. We next directed our attention to determining if FCW34 and FWC66 affect the talin−integrin signaling pathways. Integrins mediate cell adhesion to the extracellular matrix, and therefore, play an important role in cancer. Talin is a key regulator of integrin affinity and avidity.[53−55] In order to maintain integrin in an activated state, the talin N-terminal head domain must interact with the β integrin cytoplasmic tail.[56,57] In order to determine if *N*-glycan sialyation affects integrin-dependent signaling, we used FCW34 and FCW66 to inhibit the sialyltransferases and immunofluorescence and coimmunoprecipitation (Co-IP) assays to monitor the integrin−talin association events. The results obtained and reported in Figure 4A,B indicates that FCW34 and FCW66 significantly reduce colocalization of integrins β1 and β3 and phospho-talin-1 (*p*-talin-1) in MDA-MB-231 cells. Figure 4C,D shows that FCW34 and FCW66 decrease *p*-talin-1 association with integrins β1 and β3 in a dose-dependent manner. We interpret these findings to support the proposal that FCW34 and FCW66 induce the reduction of *N*-glycan sialylation and talin phosphorylation and that this might be critical for the disruption of talin-driven integrin activation and clustering, and thus, for the suppression of cancer metastasis.

FCW34 and FCW66 Decrease Cell Migration Ability through Inhibition of Talin/Integrin/FAK/Paxillin and Integrin/NFκB Signaling Pathways. In light of the importance of ECM/integrin-directed cell behavior,[58−60] we investigated whether the inhibitor induced the decrease in the migration ability of cells, and therefore, the reduction of tumor progression and angiogenesis in mice resulted from the suppression of talin/integrin/FAK/paxillin signaling or integrin/NFκB signaling.[61−64] As shown in the images reported in Figure S9A, the exposure of MDA-MB-231 cells to FCW34 and FCW66 (0, 10, and 20 μM) results in significant decreases in the expression levels of integrin isoforms (α_v, α_5, β_1, β_3, β_4, and β_5). Tyrosine (i.e., Tyr397, Tyr576, Tyr577, and Tyr925)-phosphorylated focal adhesion kinase (*p*-FAK) (Tyr397, Tyr576, Tyr577, and Tyr925) and Tyr118-phosphorylated paxillin (*p*-paxillin) were found to be reduced in a dose-dependent manner by treatment of cells with FCW34 or FCW66 (Figure S9B). In addition, FCW34 and FCW66 effectively inhibited phosphorylated *p*-IKKα/β, *p*-IκBα, and *p*-NF-κB (Figure S10), demonstrating that FCW34 and FCW66 regulate the talin/integrin/FAK/paxillin and integrin/NFκB signaling pathways and suppress breast cancer growth and angiogenesis in vivo.

In order to evaluate the efficiency of the compound permeability into cells, a parallel artificial membrane permeability assay (PAMPA) model was performed.[65,66] FCW34 and FCW66 were tested by the PAMPA method (pH = 7.4) in line with reference compounds, chloramphenicol (high permeability), diclofenac (medium permeability), and theophylline (low permeability), at 200 μM concentrations. Apparent permeability (P_{app}) values were 8.8 ± 0.2 × 10^{-6}, 7.1

https://dx.doi.org/10.1021/acs.jmedchem.0c01477
J. Med. Chem. 2021, 64, 527−542

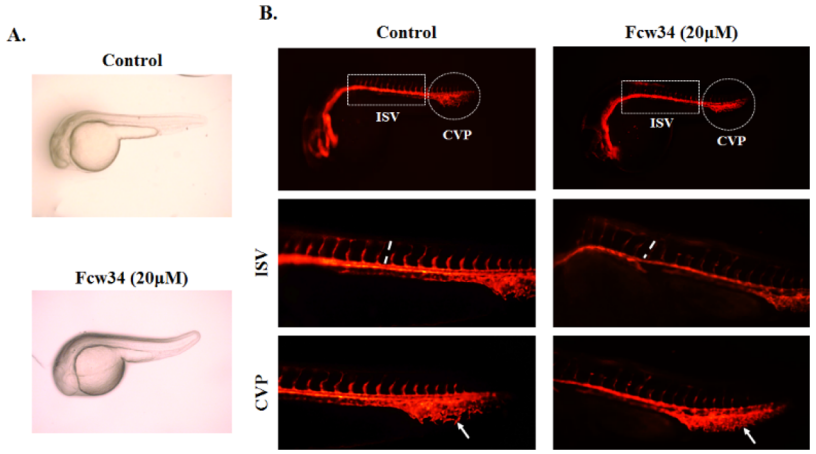

Figure 5. Effect of Fcw34 on vessel development in transgenic zebrafish models. The influence of Fcw34 (20 μM) application on blood vessel development in *Tg(kdrl:mCherry)*^{ci5} × *Tg(fli1a:negfp)*^{y7} zebrafish embryos was analyzed at various time intervals. (A) Bright-field images of Fcw34-treated embryos; (B) fluorescence microscopy analysis of Fcw34-treated embryos at 30 h postfertilization (hpf). Upper panels show the anatomical locations of ISV and CVP for observation; middle panel shows the measurements of ISV length (corresponding to the boxed area in the upper panel) in control and Fcw34-treated embryos. The sprouting length of ISV in embryos (n = 10 per group) was analyzed at 30 hpf. Data were mean ± SEM of triplicate experiments; bottom panels highlight the morphology and neovascularization in CVP morphology, as indicated by arrows.

$\pm$ 0.5 × 10^{-6}, 1.4 $\pm$ 0.1 × 10^{-6}, 3.6 $\pm$ 0.3 × 10^{-6}, and 9.0 $\pm$ 0.4 × 10^{-6} cm/s for chloramphenicol, diclofenac, theophylline, FCW34, and FCW66, respectively (Figure S11). In general, compounds with P_{app} values between 1.1 × 10^{-6} and 1.0 × 10^{-5} are mostly considered to have better pharmacokinetic characteristics. Obviously, the P_{app} values of FCW34 and FCW66 are within this range and FCW66 exhibited a 2−3-fold permeability potency increase over FCW34, indicating that FCW 66, possessing one more ethylene glycol unit of the cyclopentane ring side chain, facilitates the passive permeability.

FCW34 Is Associated with Antiangiogenesis Progression in a Zebrafish Model. To further validate the antiangiogenic activities of FCW34, we employed *Tg(kdrl:mCherry)*^{ci5} × *Tg(fli1a:negfp)*^{y7} zebrafish embryos for monitoring the neovascularization status in the intersegmental vessels (ISV) and caudal vein plexus (CVP).[67] Treatment with FCW34 did not elicit a noticeable defect in the gross morphology of zebrafish embryos (Figure 5A). However, FCW34 treatment clearly perturbed the ISV and CVP formations (Figure 5B). These results further demonstrate an underlying relationship between FCW34-induced ST inhibition and reduced angiogenic activity in vivo.

Endogenous Expression of ST6GALI, ST3GALIII, ST3GALI, and ST6GALNACI Proteins in Different Cell Lines. To indirectly evaluate the designed ST inhibitor-targeted sialyltransferases in cancer cells, we examined the existence of endogenous ST6GALI, ST3GALIII, ST3GALI, and ST6GALNACI proteins. As shown in Figure S12, the majority of cancer cell lines, MCF7, Hs578T, BT549, MDA-MB-468, MDA-MB-231, and HeLa cells, have endogenous ST6GALI, ST3GALIII, ST3GALI, and ST6GALNACI proteins. It is interesting to note that MCF7 and MDA-MB468 cells showed high levels of immunostaining for ST6GALI and ST3GALIII, respectively. In contrast, most of the cancer cell lines exhibited abundant endogenous ST3GALI and ST6GALNACI. It is important to note that the human normal epithelial cell line M10 has no detectable endogenous ST3GALIII protein but displayed higher level of immunostaining for ST6GALI compared to other cancer cell lines. This observation explains why a different cell line is associated with a distinctive level of endogenous STs. In MDA-MB231 cells, the designed ST inhibitors, FCW34 and FCW66, are able to interact with endogenous STs, which could be occasionally forced overexpression under oxidative pressure, cellular signaling, and other factors.

Physicochemical Analysis of Designed ST Inhibitors. For two decades, the rule of five (Ro5) has been widely used as the concept of drug-like properties to predict and categorize the small molecule candidates compared to oral drugs. The physicochemical parameters most commonly used are molecular weight (MW), the calculated logarithm of the water/octanol partition coefficient (clog P), number of hydrogen bond acceptors (HBA), number of hydrogen bond donors (HBD), topological polar surface area (TPSA)/molecular polar surface area (MPSA), and number of rotatable bonds (RotB). Because some FDA-approved oral drugs do not strictly obey the rule of five (Ro5), Doak and co-workers proposed reasonable outer limits for physicochemical parameters of a possible molecule to be orally absorbed.[68,69] The predicted molecular descriptors of the outer limit include MW $\leq$ 1000, −2 $\leq$ clog P $\leq$ 10, HBA $\leq$ 15, HBD $\leq$ 6, TPSA $\leq$ 250, and RotB $\leq$ 20.

The selected compounds, **2aA−2eA**, **2aB−2eB**, and **2aC−2eC**, and Taxol used in this study with the calculated parameter distributions are depicted in Supporting Information Table S1. The MW range of the selected compounds alters from 709 to 953, which is higher than that (MW $\leq$ 500) of the Ro5 hypothesis. However, the high MW compounds have reached the market recently, such as Taxol. The clog P value of the selected compounds varies from 8.5 to 10.2 compared to clog P $\leq$ 5 of Ro5 and 4.7 of Taxol, indicating that lipophilicity is too high, and a subsequent modification of the steroidal ring to reduce the lipophilic character is essential. The predicted HBA ranges from 7 to 14, and the Ro5 rule requires HBA $\leq$ 10. All the selected compounds satisfy the Ro5 hypothesis, HBD $\leq$ 5. The calculated TPSA/MPSA values fall within the range of 203−273. The RotB range of selected compounds vary from 16 to 29, which is higher than that (14) of Taxol, suggesting that the number of rotatable bonds from the PEG

https://dx.doi.org/10.1021/acs.jmedchem.0c01477
J. Med. Chem. 2021, 64, 527−542

linker and the steroidal aliphatic side chain should be reduced in order to provide an oral druggable space.

Molecular Docking. To further study the binding mode of the designed ST inhibitors, such as **2aA−2eA**, **3cB−3dB**, and **4cC−4dC** with respect to that of the reference inhibitors AL10, LCAG, and Lith-*O*-ASP in the ST6GALI structure (PDB 6QVT),[70] we built a conformation of two asymmetric polypeptide chains (A/B) of human ST6GALI structure for molecular docking, minimization, and binding energy calculations. Except ST6GALI, the crystal structure of porcine ST3GALI (2WNF) was also used to construct the donor−acceptor conformation, but it was not successful during the minimization process.[71] Simulated annealing process shows that all the protein−inhibitor complexes are stable at 700 K. On this basis, we found that the designed inhibitor complexes, **2aA−2eA**, **3cB−3dB**, and **4cC−4dC**, showed lower binding energy (−21.42 to −35.48 kcal/mol) than AL10 (−9.37 kcal/mol), LCAG (−14.73 kcal/mol), and Lith-*O*-ASP (−9.58 kcal/mol) in Table S2. This finding is consistent with the observation that **2aA−2eA**, **3cB−3dB**, and **4cC−4dC** display higher inhibitory potency than LCAG and Lith-*O*-ASP but not AL10, because there are some unfavorable bumps and unfavorable negative−negative interactions in the protein−AL10 complex. Compared with the protein−ligand structure between AL10 and **2aA**/**2bA**/**2cA**/**2dA**/**2eA**, we observed an extended space with hydrophobic and hydrophilic amino acid residues, such as P320(B), P259(B), V261(A), W302(B), H370(B), S322(B), S189(B), C353(B), G324(B), A190(B), and N212(B) in two asymmetric polypeptide chains (A/B) of ST6GALI (PDB 6QVT), where the PEG moiety of designed inhibitors might develop additional interactions. As can be seen in Figure S13, PEG moiety-containing inhibitor−protein complexes show extra key interactions involving several hydrophilic amino acid residues, S322(B), H370(B), C353(B), S189(B), D274(B), and Q235(B), indicating that these key interactions include the formation of conventional hydrogen bonding and electrostatic attraction. In addition, the shorter or longer alkyl chain (PEG linker) of the ST inhibitor seems to occupy at the similar binding pocket.

We also observed the important hydrogen-bonding interaction and a salt-bridge formation between the nitro group or nitrogen atom of NBD and Pro/Ser/Lys residues (P371(A), S323(A), S322(A), and K268(B)). Furthermore, the steroidal skeleton of **2aA−2eA**, **3cB−3dB**, **4cC−4dC**, AL10, LCAG, and Lith-*O*-ASP is well adapted to the hydrophobic cavity of ST6GALI, in which the cavity is mostly surrounded by nonpolar residues, such as P259(A), P259(B), V261(A), V261(B), Trp302(A), Trp302(B), P320(A), and P320(B). Interestingly, the azide group in the terminal of PEG chain in **2cA−2eA**, **3dB**, and **4cC** also shows a favorable hydrogen bonding or salt-bridge with neighboring amino acid residues, G324(B), S188(B), A190(B), N212(B), S189(B), or E375(B). In contrast, we did not observe any complementary binding between the azide groups of **2aA−2bA**, **3cB**, and **4dC** and ST6GALI. Overall, the increased binding affinity of ST inhibitors, **2aA−2eA**, **3cB−3dB**, and **4cC−4dC**, is primarily due to hydrogen bond formation, electrostatic attraction, or salt−bridge interaction within the binding region of protein.

CONCLUSIONS

In summary, we have designed and synthesized a series of cell-permeable and potent ST inhibitors and have demonstrated that one of these inhibitors, FCW34, markedly reduces tumor progression and angiogenesis in vivo. This represents an important step forward in ST-targeted breast cancer treatments. Furthermore, our findings suggest that the sensitization of tumors to FCW34 through manipulation of *N*-glycan sialylation, followed by regulation of the talin/integrin/FAK/paxillin and integrin/NFκB signaling pathways (Figure S14) could be a feasible therapeutic approach.

EXPERIMENTAL SECTION

Chemistry. All chemicals and reagents were commercially available and used without further purification unless indicated otherwise. All solvents were of anhydrous grade unless indicated otherwise. Reactions were monitored by thin-layer chromatography on silica gel. Flash chromatography was performed on silica gel of 60−200 μm particle size. NMR spectra were recorded on Bruker AV400, AMX400, or AV500 MHz instruments. Chemical shifts (δ) were reported in parts per million (ppm) and referenced to the chemical shift of residual solvent. High-resolution mass spectra were recorded on a Bruker Daltonics spectrometer. Chromatography was performed at room temperature using a high-performance liquid chromatography (HPLC) system consisting of a Waters 1525 Binary System with a Waters 2487 or 2489 dual λ absorbance detector, using a Kromasil 300-5C4 column (250 × 10 mm) equilibrated with 0.1% TFA/H_2O and 0.05% TFA/CH_3CN as eluents, at a flow rate of 2 mL/min, and the eluted materials were monitored using a UV absorbance detector that measured the absorbance at 254 nm, unless indicated otherwise. The HPLC fractions containing products were lyophilized in a vacuum concentrator (FreeZone plus 4.5, LABCONCO). The purity of lithocholic acid derivatives was established as >95% by employing HPLC and ^{1}H NMR spectroscopy.

*(3S)-4-(((3R,5R,8R,9S,10S,13R,14S)-17-((R)-5-(2-Azidoethoxy)-5-oxopentan-2-yl)-10,13-di-methylhexadecahydro-1H-cyclopenta-[a]phenanthren-3-yl)oxy)-3-((7-nitrobenzo[c][1,2,5] oxadiazol-4-yl)amino)-4-oxobutanoic Acid (**2aA**).* Yield: 17% (powder); mp: 78−79 °C; ^{1}H NMR (400 MHz, $CDCl_3$): δ 8.46 (d, J = 8.4 Hz, 1H), 6.97 (d, J = 8.4 Hz, 1H), 6.26 (d, J = 8.4 Hz, 1H), 4.87−4.80 (m, 2H), 4.23 (t, J = 4.8 Hz, 2H), 3.46 (t, J = 4.8 Hz, 2H), 3.21−3.06 (m, 2H), 2.42−2.34 (m, 1H), 2.29−2.21 (m, 1H), 1.95−1.89 (m, 1H), 1.86−1.75 (m, 5H), 1.67−1.64 (m, 1H), 1.55−1.52 (m, 2H), 1.50−1.29 (m, 8H), 1.28−1.20 (m, 3H), 1.16−0.97 (m, 6H), 0.91−0.88 (sd, J = 6.4 Hz, 6H),0.62 (s, 3H). ^{13}C NMR (100 MHz, $CDCl_3$): δ 174.2, 173.3, 168.6, 144.3, 143.8, 142.3, 135.7, 125.5, 100.0, 77.8, 62.9, 56.4, 55.9, 52.6, 49.8, 42.7, 41.9, 40.5, 40.1, 35.7, 35.3, 34.8, 34.6, 32.0, 31.1, 30.9, 28.1, 26.9, 26.4, 26.3, 24.2, 23.3, 20.8, 18.2, 12.0. HRMS calcd for $C_{36}H_{48}N_7O_9$ $(M - H)^-$, 722.3514; found, 722.3510.

*(3S)-4-(((3R,5R,8R,9S,10S,13R,14S)-17-((R)-5-(2-(2-Azidoethoxy)-ethoxy)-5-oxopentan-2-yl)-10,13-dimethylhexadecahydro-1H-cyclopenta[a]phenanthren-3-yl)oxy)-3-((7-nitrobenzo[c][1,2,5]-oxadiazol-4-yl)amino)-4-oxobutanoic Acid (**2bA**).* Yield: 11% (powder); mp: 75−76 °C; ^{1}H NMR (400 MHz, $CDCl_3$): δ 8.45 (d, J = 8.4 Hz, 1H), 7.02 (d, J = 7.6 Hz, 1H), 6.27 (d, J = 8.4 Hz, 1H), 44.86−4.81 (m, 2H), 4.22 (t, J = 4.8 Hz, 2H), 3.70−3.65 (m, 4H), 3.37 (t, J = 4.8 Hz, 2H), 3.20−3.05 (m, 2H), 2.40−2.33 (m, 1H), 2.27−2.19 (m, 1H), 1.94−1.91 (m, 1H), 1.86−1.73 (m, 5H), 1.67−1.64 (m, 1H), 1.54−1.52 (m, 2H), 1.44−1.29 (m, 8H), 1.27−1.19 (m, 3H), 1.15−0.97 (m, 6H), 0.90−0.86 (sd, J = 6.4 Hz, 6H), 0.61 (s, 3H). ^{13}C NMR (100 MHz, $CDCl_3$): δ 174.5, 173.5, 168.7, 144.3, 143.8, 142.3, 135.8, 125.3, 100.0, 77.7, 70.0, 69.2, 63.3, 56.4, 56.0, 52.6, 50.6, 42.7, 41.9, 40.5, 40.0, 35.7, 35.3, 34.8, 34.5, 32.0, 31.1, 30.9, 28.1, 26.9, 26.4, 26.3, 24.1, 23.2, 20.8, 18.2, 12.0. HRMS calcd for $C_{38}H_{52}N_7O_{10}$ $(M - H)^-$, 766.3776; found, 766.3767.

*(3S)-4-(((3R,5R,8R,9S,10S,13R,14S)-17-((R)-5-(2-(2-(2-Azidoethoxy)ethoxy)ethoxy)-5-oxopentan-2-yl)-10,13-dimethyl-hexadecahydro-1H-cyclopenta[a]phenanthren-3-yl)oxy)-3-((7-nitrobenzo[c][1,2,5]oxadiazol-4-yl)amino)-4-oxobutanoic Acid (**2cA; FCW34**).* Yield: 12% (powder); mp: 72−73 °C; ^{1}H NMR (400 MHz, $CDCl_3$): δ 8.46 (d, J = 8.8 Hz, 1H), 6.98 (d, J = 6.0 Hz, 1H), 6.27 (d, J = 8.8 Hz, 1H), 4.87−4.81 (m, 2H), 4.21 (t, J = 5.2 Hz, 2H), 3.71−3.66 (m, 8H), 3.38 (t, J = 5.2 Hz, 2H), 3.19−3.05 (m,

https://dx.doi.org/10.1021/acs.jmedchem.0c01477
J. Med. Chem. 2021, 64, 527−542

2H), 2.40−2.32 (m, 1H), 2.26−2.18 (m, 1H), 1.95−1.92 (m, 1H), 1.86−1.72 (m, 5H), 1.67−1.63 (m, 1H), 1.55−1.52 (m, 2H), 1.45−1.29 (m, 8H), 1.27−1.19 (m, 3H), 1.15−0.97 (m, 6H), 0.91−0.87 (sd, J = 6.4 Hz, 6H), 0.61 (s, 3H). ^{13}C NMR (100 MHz, $CDCl_3$): δ 174.5, 172.9, 168.6, 144.3, 143.8, 142.3, 135.7, 125.4, 100.0, 77.7, 70.7, 70.6, 70.1, 69.3, 63.4, 56.4, 55.9, 52.6, 50.7, 42.7, 41.9, 40.5, 40.1, 35.7, 35.3, 34.8, 34.6, 32.0, 31.9, 31.1, 30.9, 28.2, 26.9, 26.5, 26.4, 26.3, 24.2, 23.3, 20.8, 18.3, 12.0. HRMS calcd for $C_{40}H_{57}N_7O_{11}Na$ $(M + Na)^+$, 834.4014; found, 834.4014.

(3S)-4-(((3R,5R,8R,9S,10S,13R,14S)-17-((R)-1-Azido-13-oxo-3,6,9,12-tetraoxaheptadecan-16-yl)-10,13-dimethylhexadecahydro-1H-cyclopenta[a]phenanthren-3-yl)oxy)-3-((7-nitro benzo[c][1,2,5]oxadiazol-4-yl)amino)-4-oxobutanoic Acid (***2dA; FCW66***). Yield: 10% (oil); ^{1}H NMR (500 MHz, $CDCl_3$): δ 8.44 (d, J = 8.5 Hz, 1H), 7.16 (br s, 1H), 6.26 (d, J = 8.0 Hz, 1H), 4.81 (br s, 2H), 4.19 (t, J = 4.5 Hz, 2H), 3.68−3.64 (m, 12H) 3.70 (t, J = 5.0 Hz, 2H), 3.14−3.07 (m, 2H), 2.37−2.31 (m, 1H), 2.24−2.18 (m, 1H), 1.92−1.90 (m, 1H), 1.85−1.72 (m, 5H), 1.64 (br s, 1H), 1.53−1.52 (m, 2H), 1.43−1.27 (m, 8H), 1.25−1.19 (m, 3H), 1.13−0.96 (m, 6H), 0.89−0.85 (sd, J = 6.0 Hz, 6H), 0.60 (s, 3H). ^{13}C NMR (125 MHz, $CDCl_3$): δ 174.4, 172.8, 168.8, 144.3, 143.8, 142.6, 135.8, 125.2, 100.1, 77.6, 70.7, 70.6, 70.5, 70.0, 69.2, 63.4, 56.4, 55.9, 52.9, 50.7, 42.7, 41.9, 40.5, 40.1, 35.7, 35.3, 34.8, 34.6, 32.0, 31.1, 30.9, 28.1, 26.9, 26.4, 26.3, 24.1, 23.3, 20.8, 18.3, 12.0. HRMS calcd for $C_{42}H_{60}N_7O_{12}$ $(M - H)^-$, 854.4300; found, 854.4293.

(3S)-4-(((3R,5R,8R,9S,10S,13R,14S)-17-((R)-1-Azido-16-oxo-3,6,9,12,15-pentaoxaicosan-19-yl)-10,13-dimethylhexadecahydro-1H-cyclopenta[a]phenanthren-3-yl)oxy)-3-((7-nitrobenzo[c][1,2,5]-oxadiazol-4-yl)amino)-4-oxobutanoic Acid (***2eA***). Yield: 10% (oil), ^{1}H NMR (500 MHz, $CDCl_3$): δ 8.44 (d, J = 8.5 Hz, 1H), 6.26 (d, J = 7.5 Hz, 1H), 4.81 (br s, 2H), 4.20 (t, J = 4.5 Hz, 2H), 3.68−3.63 (m, 16H) 3.37 (t, J = 4.5 Hz, 2H), 3.14−3.06 (m, 2H), 2.37−2.31 (m, 1H), 2.24−2.18 (m, 1H), 1.92−1.90 (m, 1H), 1.85−1.75 (m, 5H), 1.65 (br s, 1H), 1.52−1.51 (m, 2H), 1.40−1.31 (m, 8H), 1.22−1.19 (m, 3H), 1.13−0.96 (m, 6H), 0.89−0.86 (sd, J = 6.0 Hz, 6H), 0.60 (s, 3H). ^{13}C NMR (125 MHz, $CDCl_3$): δ 174.4, 168.8, 144.3, 143.8, 142.6, 135.8, 125.1, 100.1, 77.5, 70.6, 70.5, 70.0, 69.2, 63.4, 56.5, 55.9, 53.0, 50.7, 42.7, 41.9, 40.5, 40.1, 35.7, 35.3, 34.8, 34.6, 32.0, 31.0, 30.9, 28.1, 26.9, 26.4, 26.3, 24.1, 23.2, 20.8, 18.3, 12.0. HRMS calcd for $C_{44}H_{64}N_7O_{13}$ $(M - H)^-$, 898.4562; found, 898.4556.

(3S)-4-(((3R,5R,8R,9S,10S,13R,14S)-17-((R)-5-(2-Azidoethoxy)-5-oxopentan-2-yl)-10,13-dimethylhexadecahydro-1H-cyclopenta[a]-phenanthren-3-yl)oxy)-3-(4-nitrobenzamido)-4-oxobutanoic Acid (***3aB***). Yield: 32% (powder); mp: 61−62 °C; ^{1}H NMR (400 MHz, $CDCl_3$): δ 8.29 (d, J = 8.4 Hz, 2H), 7.97 (d, J = 8.4 Hz, 2H), 7.37 (d, J = 7.6 Hz, 1H), 5.00−4.97 (m, 1H), 4.86−4.80 (m, 1H), 4.24 (t, J = 5.2 Hz, 2H), 3.47 (t, J = 5.2 Hz, 2H), 3.17 (dd, J = 17.4 Hz, 4.0 Hz, 1H), 3.06 (dd, J = 17.2 Hz, 4.0 Hz, 1H), 2.43−2.36 (m, 1H), 2.31−2.23 (m, 1H), 1.98−1.95 (m, 1H), 1.91−1.80 (m, 5H), 1.68−1.66 (m, 1H), 1.57−1.54 (m, 2H), 1.43−1.37 (m, 8H), 1.30−1.23 (m, 3H), 1.19−0.98 (m, 6H), 0.93−0.91 (sd, J = 7.6 Hz, 6H), 0.65 (s, 3H). ^{13}C NMR (100 MHz, $CDCl_3$): δ 174.0, 169.8, 165.2, 149.9, 139.1, 128.4, 123.8, 62.8, 56.4, 55.9, 49.8, 49.3, 42.7, 41.9, 40.4, 40.0, 35.7, 35.3, 34.8, 34.5, 32.0, 31.0, 30.8, 28.1, 26.9, 26.4, 26.2, 24.1, 23.2, 20.8, 18.2, 12.0. HRMS calcd for $C_{37}H_{51}N_5O_9Na$ $(M + Na)^+$, 732.3584; found, 732.3593.

(3S)-4-(((3R,5R,8R,9S,10S,13R,14S)-17-((R)-5-(2-(2-Azidoethoxy)-ethoxy)-5-oxopentan-2-yl)-10,13-dimethylhexadecahydro-1H-cyclopenta[a]phenanthren-3-yl)oxy)-3-(4-nitrobenzamido)-4-oxobutanoic Acid (***3bB***). Yield: 30% (powder); mp: 57−58 °C; ^{1}H NMR (400 MHz, $CDCl_3$): δ 8.26 (d, J = 8.8 Hz, 2H), 7.95 (d, J = 8.4 Hz, 2H), 7.34 (d, J = 6.8 Hz, 1H), 4.97−4.95 (m, 1H), 4.83−4.77 (m, 1H), 4.21 (t, J = 4.6 Hz, 2H), 3.70−3.64 (m, 4H), 3.37 (t, J = 5.2 Hz, 2H), 3.16−3.02 (m, 2H), 2.40−2.33 (m, 1H), 2.27−2.19 (m, 1H), 1.95−1.92 (m, 1H), 1.89−1.74 (m, 5H), 1.65−1.63 (m, 1H), 1.55−1.52 (m, 2H), 1.40−1.27 (m, 8H), 1.24−1.20 (m, 3H), 1.16−1.00 (m, 6H), 0.90−0.87 (sd, J = 6.4 Hz, 6H), 0.62 (s, 3H). ^{13}C NMR (100 MHz, $CDCl_3$): δ 174.4, 169.8, 165.3, 149.9, 139.1, 128.4, 123.8, 70.0, 69.2, 63.2, 56.4, 56.0, 50.6, 49.3, 42.7, 41.9, 40.4, 40.1, 35.7, 35.3, 34.9, 34.6, 32.0, 31.1, 30.9, 28.1, 26.9, 26.4, 26.3, 24.1, 23.3, 20.8, 18.3, 12.0. HRMS calcd for $C_{39}H_{55}N_5O_{10}Na$ $(M + Na)^+$, 776.3847; found, 776.3840.

(3S)-4-(((3R,5R,8R,9S,10S,13R,14S)-17-((R)-5-(2-(2-(2-Azidoethoxy)ethoxy)ethoxy)-5-oxo pentan-2-yl)-10,13-dimethylhexadecahydro-1H-cyclopenta[a]phenanthren-3-yl)oxy)-3-(4-nitro benzamido)-4-oxobutanoic Acid (***3cB***). Yield: 24% (powder); mp: 52−53 °C; ^{1}H NMR (400 MHz, $CDCl_3$): δ 8.27 (d, J = 8.8 Hz, 2H), 7.95 (d, J = 8.4 Hz, 2H), 7.36 (d, J = 7.2 Hz, 1H), 4.98−4.95 (m, 1H), 4.83−4.77 (m, 1H), 4.20 (t, J = 4.8 Hz, 2H), 3.70−3.65 (m, 8H), 3.37 (t, J = 4.8 Hz, 2H), 3.16−3.00 (m, 2H), 2.39−2.32 (m, 1H), 2.26−2.18 (m, 1H), 1.95−1.92 (m, 1H), 1.89−1.73 (m, 5H), 1.66−1.64 (m, 1H), 1.55−1.52 (m, 2H), 1.40−1.26 (m, 8H), 1.23−1.16 (m, 3H), 1.14−0.96 (m, 6H), 0.90−0.87 (sd, J = 6.4 Hz, 6H), 0.62 (s, 3H). ^{13}C NMR (100 MHz, $CDCl_3$): δ 174.4, 169.8, 165.2, 149.8, 139.1, 128.4, 123.8, 70.7, 70.6, 70.1, 69.3, 63.4, 56.4, 56.0, 50.7, 49.3, 42.7, 41.9, 40.4, 40.1, 35.7, 35.3, 34.9, 34.6, 32.0, 31.1, 30.9, 28.1, 27.0, 26.4, 26.3, 24.1, 23.3, 20.8, 18.3, 12.0. HRMS calcd for $C_{41}H_{59}N_5O_{11}Na$ $(M + Na)^+$, 820.4109; found, 820.4103.

(3S)-4-(((3R,5R,8R,9S,10S,13R,14S)-17-((R)-1-Azido-13-oxo-3,6,9,12-tetraoxaheptadecan-16-yl)-10,13-dimethylhexadecahydro-1H-cyclopenta[a]phenanthren-3-yl)oxy)-3-(4-nitro benzamido)-4-oxobutanoic Acid (***3dB***). Yield: 21% (oil); ^{1}H NMR (400 MHz, $CDCl_3$): δ 8.27 (d, J = 8.8 Hz, 2H), 7.96 (d, J = 8.4 Hz, 2H), 7.36 (d, J = 7.6 Hz, 1H), 4.7−4.96 (m, 1H), 4.80−4.79 (m, 1H), 3.72−3.58 (m, 14H), 3.38 (t, J = 4.8 Hz, 2H), 3.18−2.98 (m, 2H), 2.36−2.33 (m, 1H), 2.27−2.20 (m, 1H), 1.95−1.92 (m, 1H), 1.89−1.78 (m, 5H), 1.67−1.66 (m, 1H), 1.55−1.52 (m, 2H), 1.40−1.34 (m, 8H), 1.23−1.17 (m, 3H), 1.15−0.97 (m, 6H), 0.91−0.87 (sd, J = 4.0 Hz, 6H), 0.62 (s, 3H). ^{13}C NMR (100 MHz, $CDCl_3$): δ 175.3, 174.4, 169.9, 165.3, 149.8, 139.1, 128.5, 123.8, 72.4, 70.6, 70.5, 70.2, 70.0, 69.2, 63.4, 61.6, 56.4, 55.9, 50.6, 49.3, 42.7, 41.9, 40.4, 40.1, 36.1, 35.7, 35.4, 34.9, 34.6, 32.0, 30.9, 30.7, 28.2, 27.0, 26.3, 24.1, 23.3, 20.9, 18.3, 12.0. HRMS calcd for $C_{43}H_{63}N_5O_{12}Na$ $(M + Na)^+$, 864.4371; found, 864.4362.

(3S)-4-(((3R,5R,8R,9S,10S,13R,14S)-17-((R)-1-Azido-16-oxo-3,6,9,12,15-pentaoxaicosan-19-yl)-10,13-dimethylhexadecahydro-1H-cyclopenta[a]phenanthren-3-yl)oxy)-3-(4-nitrobenzamido)-4-oxobutanoic Acid (***3eB***). Yield: 22% (oil); ^{1}H NMR (400 MHz, $CDCl_3$): δ 8.25 (d, J = 8.4 Hz, 2H), 7.96 (d, J = 8.4 Hz, 2H), 7.44 (d, J = 6.4 Hz, 1H), 4.95 (br s, 1H), 4.78 (br s, 1H), 4.18 (t, J = 4.0 Hz, 2H), 3.63−3.62 (m, 16H), 3.35 (t, J = 4.4 Hz, 2H), 3.14−2.97 (m, 2H), 2.37−2.30 (m, 1H), 2.24−2.16 (m, 1H), 1.93−1.90 (m, 1H), 1.84−1.76 (m, 5H), 1.64−1.62 (m, 1H), 1.53−1.51 (m, 2H), 1.39−1.33 (m, 8H), 1.25−1.19 (m, 3H), 1.15−0.94 (m, 6H), 0.89−0.86 (sd, J = 6.4 Hz, 6H), 0.60 (s, 3H). ^{13}C NMR (100 MHz, $CDCl_3$): δ 174.4, 169.9, 165.2, 149.8, 139.1, 128.5, 123.8, 70.6, 70.5, 70.4, 69.9, 69.1, 63.4, 56.4, 55.9, 50.6, 49.4, 42.7, 41.9, 40.4, 40.0, 35.7, 35.3, 34.8, 34.5, 32.0, 31.1, 30.8, 28.1, 26.9, 26.4, 26.2, 24.1, 23.2, 20.8, 18.2, 12.0. HRMS calcd for $C_{45}H_{67}N_5O_{13}Na$ $(M + Na)^+$, 908.4633; found, 908.4630.

(3S)-4-(((3R,5R,8R,9S,10S,13R,14S)-17-((R)-5-(2-Azidoethoxy)-5-oxopentan-2-yl)-10,13-dimethylhexadecahydro-1H-cyclopenta[a]-phenanthren-3-yl)oxy)-3-(2-(7-methoxy-2-oxo-2H-chromen-4-yl)-acetamido)-4-oxobutanoic Acid (***4aC***). Yield: 35% (powder); mp: 151−152 °C; ^{1}H NMR (400 MHz, $CDCl_3$): δ 7.58 (d, J = 8.8 Hz, 1H), 7.31 (d, J = 7.6 Hz, 1H), 6.83 (dd, J = 8.8 Hz, 2.4 Hz, 1H), 6.73 (d, J = 2.4 Hz, 1H), 6.28 (s, 1H), 4.78−4.70 (m, 2H), 4.21 (t, J = 5.0 Hz, 2H), 3.82 (s, 3H), 3.74 (s, 2H), 3.45 (t, J = 5.0 Hz, 2H), 3.03−2.87 (m, 2H), 2.41−2.33 (m, 1H), 2.28−2.20 (m, 1H), 1.93−1.91 (m, 1H), 1.84−1.74 (m, 5H), 1.61−1.53 (m, 2H), 1.49−1.46 (m, 1H), 1.39−1.27 (m, 8H), 1.23−1.14 (m, 4H), 1.10−0.93 (m, 5H), 0.89−0.88 (sd, J = 4.4 Hz, 6H), 0.61 (s, 3H); ^{13}C NMR (100 MHz, $CDCl_3$): δ 174.3, 174.0, 169.8, 167.9, 163.0, 161.5, 155.4, 149.9, 126.0, 112.9, 112.8, 112.5, 101.0, 62.8, 56.3, 55.9, 55.8, 49.8, 49.2, 42.7, 41.9, 40.4, 40.0, 39.7, 35.8, 35.3, 34.9, 34.5, 32.0, 31.1, 30.9, 28.1, 27.0, 26.4, 26.3, 24.1, 23.3, 20.8, 18.2, 12.0. HRMS calcd for $C_{42}H_{56}N_4O_{10}Na$ $(M + Na)^+$, 799.3894; found, 799.3890.

(3S)-4-(((3R,5R,8R,9S,10S,13R,14S)-17-((R)-5-(2-(2-Azidoethoxy)-ethoxy)-5-oxopentan-2-yl)-10,13-dimethylhexadecahydro-1H-cyclopenta[a]phenanthren-3-yl)oxy)-3-(2-(7-methoxy-2-oxo-2H-chromen-4-yl)acetamido)-4-oxobutanoic Acid (***4bC***). Yield: 29%

https://dx.doi.org/10.1021/acs.jmedchem.0c01477
J. Med. Chem. 2021, 64, 527−542

(powder); mp: 142−143 °C; ^{1}H NMR (400 MHz, $CDCl_3$): δ 7.58 (d, J = 9.2 Hz, 1H), 7.30 (d, J = 7.6 Hz, 1H), 6.83 (dd, J = 8.8 Hz, 2.4 Hz, 1H), 6.73 (d, J = 2.4 Hz, 1H), 6.28 (s, 1H), 4.77−4.70 (m, 2H), 4.21 (t, J = 4.8 Hz, 2H), 3.82 (s, 3H), 3.74 (s, 2H), 3.69−3.64 (m, 4H), 3.36 (t, J = 4.8 Hz, 2H), 3.02−2.87 (m, 2H), 2.40−2.32 (m, 1H), 2.26−2.18 (m, 1H), 1.93−1.91 (m, 1H), 1.83−1.74 (m, 5H), 1.61−1.46 (m, 3H), 1.39−1.26 (m, 8H), 1.23−1.10 (m, 4H), 1.08−0.94 (m, 5H), 0.88−0.86 (sd, J = 6.0 Hz, 6H), 0.60 (s, 3H); ^{13}C NMR (100 MHz, $CDCl_3$): δ 174.3, 169.8, 167.9, 162.9, 161.5, 155.4, 149.9, 126.0, 112.9, 112.7, 112.5, 101.0, 70.0, 69.2, 63.2, 56.3, 56.0, 55.8, 50.6, 49.1, 42.7, 41.9, 40.4, 40.0, 39.7, 35.7, 35.3, 34.8, 34.5, 32.0, 31.1, 30.9, 28.1, 26.9, 26.4, 26.2, 24.1, 23.3, 20.8, 18.2, 12.0. HRMS calcd for $C_{44}H_{60}N_4O_{11}Na$ (M + Na)$^+$, 843.4156; found, 843.4147.

*(3S)-4-(((3R,5R,8R,9S,10S,13R,14S)-17-((R)-5-(2-(2-(2-Azidoethoxy)ethoxy)ethoxy)-5-oxopentan-2-yl)-10,13-dimethylhexadecahydro-1H-cyclopenta[a]phenanthren-3-yl)oxy)-3-(2-(7-methoxy-2-oxo-2H-chromen-4-yl)acetamido)-4-oxobutanoic Acid (**4cC**).* Yield: 25% (powder); mp: 134−135 °C; ^{1}H NMR (400 MHz, $CDCl_3$): δ 7.57 (d, J = 8.8 Hz, 1H), 7.36 (d, J = 7.2 Hz, 1H), 6.82 (dd, J = 8.8 Hz, 2.0 Hz, 1H), 6.72 (d, J = 2.0 Hz, 1H), 6.27 (s, 1H), 4.77−4.69 (m, 2H), 4.20 (t, J = 4.8 Hz, 2H), 3.81 (s, 3H), 3.74 (s, 2H), 3.70−3.64 (m, 8H), 3.36 (t, J = 5.2 Hz, 2H), 3.02−2.85 (m, 2H), 2.38−2.31 (m, 1H), 2.25−2.17 (m, 1H), 1.92−1.90 (m, 1H), 1.82−1.73 (m, 5H), 1.57−1.44 (m, 3H), 1.38−1.25 (m, 8H), 1.22−1.13 (m, 4H), 1.08−0.93 (m, 5H), 0.87−0.86 (sd, J = 5.2 Hz, 6H), 0.60 (s, 3H); ^{13}C NMR (100 MHz, $CDCl_3$): δ 174.4, 174.3, 169.8, 168.0, 162.9, 161.5, 155.3, 149.9, 126.0, 113.0, 112.7, 112.5, 100.9, 70.6, 70.5, 70.0, 69.2, 63.3, 56.3, 56.0, 55.7, 50.6, 49.1, 42.7, 41.9, 40.3, 40.0, 39.6, 35.7, 35.3, 34.8, 34.5, 32.0, 31.2, 30.9, 28.1, 26.9, 26.3, 26.2, 24.1, 23.2, 20.8, 18.2, 12.0. HRMS calcd for $C_{46}H_{64}N_4O_{12}Na$ (M + Na)$^+$, 887.4418; found, 887.4417.

*(3S)-4-(((3R,5R,8R,9S,10S,13R,14S)-17-((R)-1-Azido-13-oxo-3,6,9,12-tetraoxaheptadecan-16-yl)-10,13-dimethylhexadecahydro-1H-cyclopenta[a]phenanthren-3-yl)oxy)-3-(2-(7-methoxy-2-oxo-2H-chromen-4-yl)acetamido)-4-oxobutanoic Acid (**4dC**).* Yield: 21% (powder); mp: 126−127 °C; ^{1}H NMR (500 MHz, $CDCl_3$): δ 7.57 (d, J = 9.0 Hz, 1H), 7.34 (d, J = 7.5 Hz, 1H), 6.83 (dd, J = 9.0 Hz, 2.0 Hz, 1H), 6.72 (d, J = 2.0 Hz, 1H), 6.27 (s, 1H), 4.77−4.69 (m, 2H), 4.19 (t, J = 4.5 Hz, 2H), 3.82 (s, 3H), 3.74 (s, 2H), 3.68−3.64 (m, 12H), 3.36 (t, J = 4.5 Hz, 2H), 3.02−2.85 (m, 2H), 2.37−2.31 (m, 1H), 2.24−2.17 (m, 1H), 1.92−1.90 (m, 1H), 1.82−1.74 (m, 5H), 1.60−1.45 (m, 3H), 1.37−1.26 (m, 8H), 1.25−1.10 (m, 4H), 1.07−0.93 (m, 5H), 0.87−0.86 (sd, J = 6.5 Hz, 6H), 0.60 (s, 3H); ^{13}C NMR (125 MHz, $CDCl_3$): δ 174.3, 174.0, 169.8, 167.9, 163.0, 161.4, 155.4, 149.8, 126.0, 113.0, 112.7, 112.5, 101.0, 70.7, 70.6, 70.5, 70.0, 69.2, 63.4, 56.4, 56.0, 55.8, 50.7, 49.2, 42.7, 41.9, 40.4, 40.0, 39.7, 35.8, 35.3, 34.9, 34.6, 32.0, 31.2, 30.9, 28.1, 27.0, 26.4, 26.3, 24.1, 23.3, 20.8, 18.3, 12.0. HRMS calcd for $C_{48}H_{68}N_4O_{13}Na$ (M + Na)$^+$, 931.4681; found, 931.4681.

*(3S)-4-(((3R,5R,8R,9S,10S,13R,14S)-17-((R)-1-Azido-16-oxo-3,6,9,12,15-pentaoxaicosan-19-yl)-10,13-dimethylhexadecahydro-1H-cyclopenta[a]phenanthren-3-yl)oxy)-3-(2-(7-methoxy-2-oxo-2H-chromen-4-yl)acetamido)-4-oxobutanoic Acid (**4eC**).* Yield: 21% (powder); mp: 113−114 °C; ^{1}H NMR (500 MHz, $CDCl_3$): δ 7.57 (d, J = 8.5 Hz, 1H), 7.34 (d, J = 7.0 Hz, 1H), 6.82 (dd, J = 9.0 Hz, 2.0 Hz, 1H), 6.73 (d, J = 2.0 Hz, 1H), 6.27 (s, 1H), 4.75−4.71 (m, 2H), 4.18 (t, J = 5.0 Hz, 2H), 3.81 (s, 3H), 3.73 (s, 2H), 3.67−3.62 (m, 16H), 3.35 (t, J = 5.0 Hz, 2H), 3.01−2.85 (m, 2H), 2.37−2.31 (m, 1H), 2.23−2.17 (m, 1H), 1.92−1.90 (m, 1H), 1.79−1.73 (m, 5H), 1.59−1.44 (m, 3H), 1.35−1.26 (m, 8H), 1.25−1.10 (m, 4H), 1.07−0.92 (m, 5H), 0.87−0.85 (sd, J = 6.5 Hz, 6H), 0.59 (s, 3H); ^{13}C NMR (125 MHz, $CDCl_3$): δ 174.2, 169.8, 167.9, 162.9, 161.3, 155.4, 149.7, 126.0, 113.1, 112.7, 112.5, 101.0, 76.6, 70.7, 70.6, 70.6, 70.5, 70.0, 69.2, 63.4, 56.3, 56.0, 55.7, 50.7, 49.2, 42.7, 41.9, 40.4, 40.0, 39.7, 35.8, 35.3, 34.9, 34.5, 32.0, 31.2, 30.9, 28.1, 26.9, 26.4, 26.3, 24.1, 23.2, 20.8, 18.3, 12.0. HRMS calcd for $C_{50}H_{72}N_4O_{14}Na$ (M + Na)$^+$, 975.4943; found, 975.4945.

Biology. Human ST6GAL1 was purchased from R&D systems (#7620-GT) at specific activity >150 pmol/min/μg, stored at −80 °C, and used within 1 week. Rat ST3GAL3 (CalBiochem #566218) and rat ST3GALI (CalBiochem #566227) were obtained from CalBiochem at specific activities of 2.4 and 7.0 U/mg, respectively, stored at −80 °C, and consumed within 1 week. The donor substrate, CMP-Neu5Ac (Sigma #C8271), and acceptors, *p*-nitrophenyl T-antigen (Calbiochem #575303) and Galβ1-4GlcNAc (*N*-acetyllactosamine, Calbiochem, Millipore 345250), were purchased from commercially available vendors.

α2,3-O-Sialyltransferase (α2,3-O-ST) Inhibition Assay.[26,28] For detection of sialyltransferase activity, reverse-phase HPLC was applied to detect the end product of sialylated saccharides. The assay mixtures contained the following components: 200 mM MES buffer; 100 mM NaCl; 0.5 mM EDTA; 0.01% Triton X-100; 1.4 mU ST3GALI; 2.5 mM *p*-nitrophenyl T-antigen; 1 mM CMP-Neu5Ac; and different concentrations of sialyltransferase inhibitors to a total volume of 50 μL. The assay mixture was incubated at 37 °C for 15 min and then quenched by heating up to 101 °C for 10 min. The sialylated product was resolved by reversed-phase HPLC. For the IC_{50} value, we chose six to eight concentrations of compounds within the range of 0 to 100% inhibition in response to enzyme activity. The internal standard (acceptor or sialylated product) was used to improve the precision of quantitative analysis in HPLC. The residual activities (%) versus compound concentrations were plotted to fit the sigmoidal curve (or the dose−response curve) equations, and the IC_{50} values were calculated using GraphPad Prism software. Kinetic data were obtained by fitting the initial rate data to the nonlinear regression equation.

α2,3-N-Sialyltransferase (α2,3-N-ST) Inhibition Assay.[26] For the detection of sialyltransferase activity, the reverse-phase HPLC was applied to detect the end product of sialylated saccharides. The assay mixtures contained the following components: 200 mM MES buffer; 100 mM NaCl; 0.5 mM EDTA; 0.01% Triton X-100; 1.4 mU ST3GALIII; 25 μM Galβ1-4Glc; 1mM CMP-Neu5Ac; and different concentrations of test compounds to a total volume of 50 μL. The assay mixture was incubated at 37 °C for 1.5 h and then quenched by heating up to 101 °C for 10 min. The sialylated product was identified and analyzed by reversed-phase HPLC. For the IC_{50} value, we chose six to eight concentrations of compounds within the range of 0 to 100% inhibition in response to enzyme activity. The internal standard (acceptor or sialylated product) was used to improve the precision of quantitative analysis in HPLC. The residual activities (%) versus compound concentrations were plotted to fit the sigmoidal curve (or the dose−response curve) equations, and the IC_{50} values were calculated using GraphPad Prism software. Kinetic data were obtained by fitting the initial rate data to the nonlinear regression equation.

α2,6-N-Sialyltransferase (α2,6-N-ST) Inhibition Assay.[26] For detection of sialyltransferase activity, the reverse-phase HPLC was applied to detect the end product of sialylated saccharides. The assay mixtures contained the following components: 25 mM Tris buffer; 150 mM NaCl; 5 mM $CaCl_2$; 10 mM $MnCl_2$; 0.5 μg ST6GALI; 25 μM Galβ1-4GlcNAc; 1 mM CMP-Neu5Ac; and different concentrations of sialyltransferase inhibitors to a total volume of 50 μL. The assay mixture was incubated at 37 °C for 15 min and then quenched by heating up to 101 °C for 10 min. The sialylated product was resolved by reversed-phase HPLC. For the IC_{50} value, we chose six to eight concentrations of compounds within the range of 0 to 100% inhibition in response to enzyme activity. The internal standard (acceptor or sialylated product) was used to improve the precision of quantitative analysis in HPLC. The residual activities (%) versus compound concentrations were plotted to fit the sigmoidal curve (or the dose−response curve) equations, and the IC_{50} values were calculated using GraphPad Prism software. Kinetic data were obtained by fitting the initial rate data to the nonlinear regression equation.

Cell Culture. Human breast carcinoma MDA-MB-231, MCF-7, and Hs 578T cells were purchased from Bioresource Collection and Research Center (BCRC 60425, 60436 and 60120, respectively) and maintained in Dulbecco's modified Eagle's medium (DMEM; HyClone) with 10% fetal bovine serum (FBS; Biological Industries), 2 mM L-glutamine, and antibiotics (containing 100 mg/L Streptomycin and 100 U/mL Penicillin G). Hs 578T was supplemented with 10 μg/mL bovine insulin (Sigma) additionally. All the cell lines were maintained in a humidified incubator with 5%

https://dx.doi.org/10.1021/acs.jmedchem.0c01477
J. Med. Chem. 2021, 64, 527−542

CO_2 at 37 °C. The mammary epithelial M10 cell line was purchased from Bioresource Collection and Research Center (BCRC 60197) and maintained in the Minimum Essential Medium (MEM; Gibco BRL) with 10% FBS (Biological Industries), 2 mM L-glutamine, and antibiotics (containing 100 mg/L Streptomycin and 100 U/mL Penicillin G). Cell lines were maintained in a humidified incubator with 5% CO_2 at 37 °C. The human breast carcinoma MDA-MB-468 cell line was purchased from American Type Culture Collection (ATCC HTB-132) and maintained in Leibovitz's L-15 Medium (Gibco; 11415-064) with 10% FBS (Biological Industries), 2 mM L-glutamine, and antibiotics (containing 100 mg/L Streptomycin and 100 U/mL Penicillin G). Cell lines were maintained in a humidified incubator at 37 °C. The human breast carcinoma BT-549 cell line was purchased from American Type Culture Collection (ATCC HTB-122) and maintained in the RPMI-1640 medium (Hyclone; SH30027.02) with 10% FBS (Biological Industries), 0.023 U/mL insulin (Sigma), 2 mM L-glutamine, and antibiotics (containing 100 mg/L Streptomycin, 100 U/mL Penicillin G). Cell lines were maintained in a humidified incubator with 5% CO_2 at 37 °C. Human cervical adenocarcinoma HeLa cells were purchased from American Type Culture Collection (ATCC CCL-2) and maintained in DMEM (HyClone) with 10% FBS (Biological Industries), 2 mM L-glutamine, and antibiotics (containing 100 mg/L Streptomycin and 100 U/mL Penicillin G). Cell lines were maintained in a humidified incubator with 5% CO_2 at 37 °C.

Western Blot. Samples containing equal amounts of protein (30 μg) were separated on a 6 to 10% SDS-PAGE and electroblotted onto Immobilon-P membranes (Millipore Corp.) in a transfer buffer. Immunoblotting was performed using antibodies against talin-1, FAK, paxillin, IKKα, IKKβ, NFκB, IκBα, β-tubulin (Cell signaling), phospho-talin, phospho-FAK (Tyr 397) (Tyr 576/577) (Tyr925), phospho-IKKα/β, phospho-NFκB, phospho-IκBα, phospho-paxillin (Cell Signaling), ST3GALIII (Santa Cruz), β-actin (BD Biosciences), and secondary antibodies antimouse IgG and antirabbit IgG (Perkin Elmer). The antibody reaction was visualized using SuperSignal West Pico reagent (Thermo Scientific).

Detection of Endogenous Sialyltransferase Expression by Western Blot Analysis. To understand the endogenous ST expression levels in M10, MCF7, Hs578T, BT549, MDA-MB-468, MDA-MB-231, and HeLa cell lines. Cells were harvested and lysed with cell lysis buffer (Cell Signaling Technology). Protein concentrations were determined and equalized before loading. Samples containing equal amounts of protein (20 μg) were separated on 10% SDS-PAGE gel and electroblotted onto a polyvinylidene fluoride-transfer membrane (PVDF, Pall Corporation) in a transfer buffer. Immunoblotting was performed using specific antibodies including ST6GALI (Thermo Fisher Scientific; #MA5-11900), ST6GALNACI (Thermo Fisher Scientific; #PA5-31200), ST3GALIII (Santa Cruz Biotechnology; #sc-134040), ST3GALI (GeneTex; #*GTX106121*), and β-actin (EMD Millipore; #MAB1501) as internal control. The antibody reaction was visualized by the western blot chemiluminescence reagent (PerkinElmer) using an FL1000 imaging system.

MTT Cytotoxicity Assay. About 10^4 of MDA-MB-231 cells were seeded on 96-well culture dishes in DMEM (Gibco) containing 10% FBS (Gibco). Different concentrations of compounds were added to each plate and incubated for 48 h. Cell viabilities at different concentrations of compounds-−treatments were determined by the 3-(4,5-dimethylthiazol-2-yl)-2,5-diphenyl tetrazolium bromide (MTT, Sigma) assay. In the untreated control, 0.1% DMSO-containing medium was used.

Transwell Migration Assay. The cell migration assay was performed using transwell chambers with a filter insert (8 μm pore; Falcon, BD Biosciences). Cells were seeded onto the transwell insert with a serum-free medium at a density of 8×10^4 cells/mL and then treated with different doses of sialyltransferase inhibitors or DMSO for 16 h. Conditioned medium obtained from 5% fetal bovine serum in tissue culture medium was added to the lower wells as a chemoattractant. Thereafter, invading cells were fixed and stained after 16 h. These experiments were carried out in triplicate. Three random views were photographed and the mean number of invasive cells was counted under a microscope.

Transient Transfection of siRNA Against ST3GALIII. STEALTH siRNA against human ST3GALIII was purchased from Thermo Fisher; the sequences are shown in Table 2.

Table 2

siRNA ID	name	sequence
HSS143938	siST3GalIII (A)	GGA CGC ACA AUA UCC AGC GAG AGA A
		UUC UCU CGC UGG AUA UUG UGC GUC C
HSS143939	siST3GalIII (B)	GGA AGC UGG UGA AAG CUC GCG UCA U
		AUG ACG CGA GCU UUC ACC AGC UUC C
HSS143940	siST3GalIII (C)	GGG ACU CUU GGU AUU UGU GCG CAA U
		AUU GCG CAC AAA UAC CAA GAG UCC C

Human breast cancer cells MDA-MB-231 were seeded onto 6-well plates to 40−60% confluency. The siRNA against human ST3GALIII (Invitrogen) was dissolved in DEPC water to form 20 μM solutions. The lipofectamine RNAiMAX transfection reagent was diluted in Opti-MEM medium. siRNA was also diluted in Opti-MEM medium, mixed with the lipofectamine RNAiMAX reagent in a 1:1 ratio, and then added to cells. After 72 h, cells were harvested for further analysis.

Real-Time PCR. RNA was isolated from MDA-MB-231 cells using the PureLink RNA Mini Kit (Ambion Inc.) according to manufacturer's instructions. For reverse transcription, 5 μg of total RNA was used for reverse transcription with Superscript III (Invitrogen Co.) using olio-dT and random primers. One-twentieth of reverse-transcription products were used as a template for real-time PCR in iQ5 (BioRad) using a SYBR Green I assay. PCR was performed in 20 μL of SYBR Green PCR Master Mix (Thermo) containing 0.5 μM forward primers and reverse primers, and approximately 30 ng of cDNA. Amplification and detection were performed as follows: 1 cycle of 95 °C for 10 min, 40 cycles of 95 °C for 5 s, 62 °C for 5 s, and 72 °C for 10 s. The primer sequences for Human ST3GALIII were the following: the forward primer 5′-TAGCCCTCTGCCTCTTTCT-3′ and the reverse primer 5′-TTGCGTACTTGGTGGCTAAT-3′, which amplified a 204-bp ST3GALIII cDNA fragment. The β-actin mRNA level was determined using the following: the forward primer 5′-TCACCCA-CACTGTGCCTATCTACGA-3′ and the reverse primer 5′-CAGCG-GA ACCGCTCATTGCCAATGG-3′, which amplified a 295-bp β-actin cDNA fragment.

Lectin Affinity Assay and IP-Western Blotting. The lectin affinity assay was modified according to the previous study reported.[1] The cell surface α-2,3-sialylated antigen-expressing proteins were specifically captured using biotinylated *Maackia amurensis* Lectin II (MALII) (Vector Laboratories, Inc.) About 500 μg of total cell lysate proteins were incubated with MALII for 16 h at 4 °C with rotation. The MALII−protein complexes were captured using Streptavidin-conjugated agarose beads, followed by washing with RIPA buffer three times. Antigen-expressed proteins were released into the SDS-PAGE sample buffer and immunoblotted with target protein integrin-β_1, -β_3, -β_4, and -β_5 (Cell Signaling, Inc.).

Immunofluorescence Assay. Cells were cultured on cover slides and treated without or with Fcw34 and Fcw66 (10 and 20 μM) for 48 h. Cells were fixed with 4% paraformaldehyde for 5 min at 4 °C. After fixation, cells were permeabilized by 0.3% Triton X-100 at room temperature for 30 min, followed by blocking with 2% BSA for 30 min. Cells were probed with the rabbit-antiphospho-talin antibody (1 mg/mL) and mouse-anti-integrin β_1 or integrin β_3 at 4 °C O/N, followed by Alexa405-labeled goat-antimouse and Alexa546-labeled goat-antirabbit secondary antibodies. DRAQ7 (Abcam) was used for

https://dx.doi.org/10.1021/acs.jmedchem.0c01477
J. Med. Chem. 2021, 64, 527−542

counter staining. Finally, slides were mounted using the Fluoromount-G reagent and observed under a fluorescence microscope (Zeiss LSM 780 plus ELYRA S.1, Germany).

Immunoprecipitation Assay. Cells were lysed in RIPA buffer (20 mM Tris-HCl, 150 mM NaCl, 1 mM Na_2EDTA, 1 mM EGTA, 1% NP-40, 1% sodium deoxyphosphate, 2.5 mM pyrophosphate, 1 mM β-glycerophosphate, 1 mM Na_3VO_4, 1 μg/mL Leupeptin, and 1 mM PMSF). After clarification, 800 μg of total proteins was immunoprecipitated with the antibody to *p*-talin-1 (Cell Signaling, Inc.) and protein A Dynabeads (Life Technology, Inc.). Immunoprecipitates were subjected to Western blotting using the indicated antibodies.

Xenograft Study. Athymic nude mice (BALB/cAnN.Cg-*Foxn1*^{nu}/CrlNarl) of 4−5 weeks of age were obtained from the National Laboratory Animal Center (Taipei, Taiwan) and were raised in a specific pathogen-free environment. The animal studies were approved by the Animal Core Facility at Academia Sinica.

The breast cancer MDA-MB-231/Luc cells were kindly provided by Dr. Pei-wen Hsiao (ABRC Laboratory Animal Core Facility, Agricultural Biotechnology Research Center, Academia Sinica, Taipei); first, they were re-suspended in normal saline and then subcutaneously injected into the abdominal mammary gland area of nude mice. Tumor volumes and body weight were measured every week and calculated using the formula, $V = 1/2 \times \text{length} \times (\text{width})^2$. While the tumor grew to about 70−100 mm^3 (Day 20), we divided the animals into two groups randomly and all mice received 10 mg/kg FCW34 every other day. Vehicle (40% PEG400 + 60% normal saline) treatment was used as control. The growth and spontaneous metastasis of tumors were observed under an IVIS50 in vivo imaging system (Xenogen) with Firefly D-Luciferin substrate (NanoLight) injection. The metastasized tumor tissues were dissected on day 56.

Ethics Statement. The procedures of animal experiments were performed according to the guidelines provided by the Council of Agriculture Executive Yuan, Taiwan (ROC). The protocol used for the mouse study was approved by the Academia Sinica Institutional Animal Care and Use Committee (Protocol ID 11-12-297) and conducted in accordance with the guidelines. The mice were raised in a specific pathogen-free environment and efforts were made to minimize animal suffering.

Histological Analysis. Tissues were fixed in either 4% paraformaldehyde or Bouin's solution for 24 h following standard sectioning methods and staining in hematoxylin/eosin.

Immunohistochemistry. The paraffin-embedded tissue blocks were sectioned into 3 μm slices and mounted on the poly-L-lysine-coated slides. After deparaffinization, the slides were blocked with 3% hydrogen peroxide for 10 min and subjected to antigen retrieval with microwaving in 10 mM citrate buffer for 15 min. The CD31 (1:100 dilution; BD) and Ki67 (1:200 dilution; Novocastra) antibodies were applied onto the sections and incubated at 4 °C overnight, followed by repeated wash with phosphate-buffered saline (PBS). The horseradish peroxidase/Fab polymer conjugate (Polymer Detection System, Zymed, USA) was then applied to the sections and the sections were incubated for 30 min. After rinsing with PBS, the sections were incubated with the peroxidase substrate diaminobenzidine (1:20 dilution, Zymed) for 5 min. Thereafter, the sections were counterstained with Gill's hematoxylin for 2 s, dehydrated with serial dilutions of ethyl alcohol, cleared with xylene, and finally mounted.

Parallel Artificial Membrane Permeability Assay. The assay was performed as described in the protocol of the parallel artificial permeability assay kit (Bioassay Systems, PAMPA-096). Working solutions of each compound were prepared from 10 mM stock solution in DMSO, which was then diluted into a final concentration of 200 μM PBS (pH 7.4, 2% DMSO). Solution containing 5% lecithin/dodecane was added to the donor side of the well membrane. Reference compounds, chloramphenicol, diclofenac, and theophylline, with 200 μM concentrations were chosen as the permeability control and the test compounds (200 μM), FCW34 and FCW66, were then added to duplicate the donor wells. The acceptor side of the well was filled with PBS. The plates were then kept at room temperature for 18 h. On the following day, samples were collected from the acceptor sides. The acceptor solution, equilibrium standard (200 μM permeability control and the test compound), and blank control solutions were then added to wells of UV plates (Thermo Fisher Scientific, #8404). UV absorption was measured from 230 to 500 nm in 10 nm intervals to determine the peak absorbance of the control and test compounds (Enspire Multimode Plate Reader, PerkinElmer). The apparent permeability (P_{app}) and permeability rate (Pe) values were calculated using the determined peak absorbance for each respective test compound and permeability control.

Zebrafish Angiogenesis Model. Zebrafish (*Daniorerio*) transgenic lines *Tg(kdrl:mCherry)ci*^{5} × *Tg(fli1a:negfp)y*^{72,3} were from Taiwan Zebrafish Core Facility (Academia Sinica, Taipei, Taiwan) and maintained at 28.5 °C in an incubator with approval from the Animal Care Committee at National Sun Yat-sen University (Kaohsiung, Taiwan). Embryos were treated with 0.003% 1-phenyl-2-thiourea (PTU; Sigma, St. Louis, MO, USA) at 6 h postfertilization (hpf) to prevent pigment formation and used to monitor the effects of Fcw34 on embryonic angiogenesis.[4] Zebrafish embryos were generated by natural pair-wise mating and raised at 28 °C in embryo water (0.2 g/L of Instant Ocean Salt in distilled water). Approximately, 20 healthy embryos were placed in 6 cm dishes and various concentrations of Fcw34 were separately added to the embryo water at 6 h postfertilization (hpf). The embryo water containing Fcw34 was replaced daily. At 30 hpf, the embryos were anesthetized using 0.05% 2-phenoxyethanol in embryo water and examined for vessel development, especially in the ISV and the CVP; at 48 hpf, the migration and proliferation of endothelial cells were observed in the ISV, using a fluorescence microscope with a digital imaging system (Olympus; Tokyo, Japan). The length of the ISV was measured with the NIH Image program.

Statistical Analysis. Differences between the groups were statistically evaluated using the unpaired Student's *t*-test. The results are presented as mean ± SEM. All *P* values were two-tailed, and a *P* value of less than 0.05 was considered to be statistically significant.

■ ASSOCIATED CONTENT

Supporting Information

The Supporting Information is available free of charge at https://pubs.acs.org/doi/10.1021/acs.jmedchem.0c01477.

Effect of **2aA−2eA** on migration in MDA-MB-231 cells; effect of FCW34 on migration in MDA-MB-231 cells; effect of FCW66 on migration in MDA-MB-231 cells; effects of ST3GALIII siRNA knockdown efficiency in MDA-MB-231 cells; inhibition of integrin sialylation by sialyltransferase inhibitors in MDA-MB-231 cells; effects of sialyltransferase inhibitor FCW34 on tumor metastasis in MDA-MB-231 breast cancer cells in vivo; effects of sialyltransferase inhibitor FCW34 on toxicity assessment in MDA-MB-231 breast cancer cells in vivo; effects of sialyltransferase inhibitors on the integrin−FAK−paxillin pathway in MDA-MB-231 cells; effects of sialyltransferase inhibitors on the NFκB pathway in MDA-MB-231 cells; apparent permeability (P_{app}) values obtained for the reference compounds, FCW34, and FCW66 using the PAMPA model; endogenous expression of ST6GALI, ST3GALIII, ST3GALI, and ST6GALNACI proteins; comparison of binding modes of **2aA−2eA**, **3cB−3dB**, **4cC−4dC**, AL10, LCAG, and Lith-*O*-ASP in the binding sites of two asymmetric polypeptide chains (A/B) of ST6GALI (PDB 6QVT); computed physicochemical properties of the selected compounds used in this study; computational binding values of complex structure of ST6GALI-inhibitor; sensitization of tumors to ST inhibitors by regulation of the talin/integrin/FAK/paxillin and integrin/NFκB-signaling pathways; and experimental procedures, details

https://dx.doi.org/10.1021/acs.jmedchem.0c01477
J. Med. Chem. 2021, 64, 527−542

of HPLC-determined purity data, HRMS results, and ^{1}H and ^{13}C NMR spectra of all final compounds and intermediates (PDF)

Molecular formula strings and some data (CSV)

AUTHOR INFORMATION

Corresponding Author

Wen-Shan Li − *Institute of Chemistry, Academia Sinica, Taipei 115, Taiwan; Doctoral Degree Program in Marine Biotechnology, National Sun Yat-Sen University, Kaohsiung 804, Taiwan; Ph.D Program in Biotechnology Research and Development, Taipei Medical University, Taipei 110, Taiwan; Department of Medicinal and Applied Chemistry, Kaohsiung Medical University, Kaohsiung 807, Taiwan; Department of Chemistry, College of Science, Tamkang University, New Taipei City 251, Taiwan;* orcid.org/0000-0002-8359-4582; Email: wenshan@gate.sinica.edu.tw

Authors

Chih-Wei Fu − *Institute of Chemistry, Academia Sinica, Taipei 115, Taiwan; Department of Chemistry, National Central University, Taoyuan City 320, Taiwan*

Han-En Tsai − *Institute of Chemistry, Academia Sinica, Taipei 115, Taiwan*

Wei-Sheng Chen − *Institute of Chemistry, Academia Sinica, Taipei 115, Taiwan; Department of Chemistry, National Central University, Taoyuan City 320, Taiwan*

Tzu-Ting Chang − *Institute of Chemistry, Academia Sinica, Taipei 115, Taiwan*

Chia-Ling Chen − *Institute of Chemistry, Academia Sinica, Taipei 115, Taiwan*

Pei-Wen Hsiao − *Agricultural Biotechnology Research Center, Academia Sinica, Taipei 115, Taiwan*

Complete contact information is available at: https://pubs.acs.org/10.1021/acs.jmedchem.0c01477

Author Contributions

C.-W.F., H.-E.T., W.-S.C., T.T.-C., and C.-L.C. designed and performed the experiments. H.-E.T., C.-L.C., and P.-W.H. analyzed and interpreted the data. W.-S.L. conceived, designed, and directed the project and wrote the manuscript. C.-W.F. and H.-E.T. contributed equally as the first author.

Notes

The authors declare no competing financial interest.

ACKNOWLEDGMENTS

We acknowledge the use of NMR and Mass Spectrometry facilities of the Institute of Chemistry at Academia Sinica, Taiwan. Instrumentation support was provided by the Chemical Biology Facility of the Institute of Chemistry at Academia Sinica, Taiwan. We thank the Academia Sinica Advanced Optics Microscope Core Facility for microscopy imaging technical support. The core facility was funded by the Academia Sinica Core Facility and the Innovative Instrument Project (AS-CFII-108-116). We are grateful for financial support for this study provided by Academia Sinica (AS-SUMMIT-109 and AS-KPQ-109-BioMed) and the Ministry of Science and Technology (MOST, Taiwan, NSC 101-2325-B-001-025, NSC 102-2325-B-001-025, MOST 103-2325-B-001-001, MOST 106-2113-M-001-011, MOST 108-2113-M-001-020, MOST 108-3111-Y-001-056, and MOST-108-3114-Y-001-002).

ABBREVIATIONS

ASP, aspartic acid; CD31, cluster of differentiation 31; Co-IP, coimmunoprecipitation; CVP, caudal vein plexus; DBU, 1,8-diazabicyclo[5.4.0]undec-7-ene; DCC, dicyclohexylcarbodiimide; DIPEA, *N*,*N*-diisopropylethylamine; DMAP, 4-(dimethylamino)pyridine; EC, ethylene glycol; ECM, extracellular matrix; FAK, focal adhesion kinase; FMOC, fluorenylmethoxycarbonyl; HBTU, 2-(1*H*-benzotriazol-1-yl)-1,1,3,3-tetramethyluronium hexafluorophosphate; HPF, hours postfertilization; H&E, hematoxylin and eosin; IKK, inhibitory kappa B kinase; ISV, intersegmental vessels; LCA, lithocholic acid; MC, methoxycoumarin; NBD, *N*-nitrobenzoxadiazole; NF-κB, nuclear factor kappa-light-chain-enhancer of activated B cells; PECAM-1, platelet-endothelial cell adhesion molecule-1; PEG, polyethylene glycol; ST, sialyltransferase; *t*-BU, *tert*-butyl; TFA, trifluoroacetic acid

REFERENCES

(1) Cheung, K. J.; Ewald, A. J. A Collective Route to Metastasis: Seeding by Tumor Cell Clusters. *Science* **2016**, *352*, 167−169.

(2) Comen, E.; Norton, L.; Massagué, J. Clinical Implications of Cancer Self-Seeding. *Nat. Rev. Clin. Oncol.* **2011**, *8*, 369−377.

(3) Fidler, I. J. The Pathogenesis of Cancer Metastasis: The 'Seed and Soil' Hypothesis Revisited. *Nat. Rev. Cancer* **2003**, *3*, 453−458.

(4) Zhang, Z.; Wuhrer, M.; Holst, S. Serum Sialylation Changes in Cancer. *Glycoconjugate J.* **2018**, *35*, 139−160.

(5) Bhide, G. P.; Colley, K. J. Sialylation of N-Glycans: Mechanism, Cellular Compartmentalization and Function. *Histochem. Cell Biol.* **2017**, *147*, 149−174.

(6) Büll, C.; Stoel, M. A.; den Brok, M. H.; Adema, G. J. Sialic Acids Sweeten a Tumor's Life. *Cancer Res.* **2014**, *74*, 3199−3204.

(7) Yogeeswaran, G.; Salk, P. Metastatic Potential Is Positively Correlated with Cell Surface Sialylation of Cultured Murine Tumor Cell Lines. *Science* **1981**, *212*, 1514−1516.

(8) Toegel, S.; Pabst, M.; Wu, S. Q.; Grass, J.; Goldring, M. B.; Chiari, C.; Kolb, A.; Altmann, F.; Viernstein, H.; Unger, F. M. Phenotype-related Differential Alpha-2,6- or Alpha-2,3-sialylation of Glycoprotein N-glycans in Human Chondrocytes. *Osteoarthr. Cartil.* **2010**, *18*, 240−248.

(9) Chung, C.-Y.; Yin, B.; Wang, Q.; Chuang, K.-Y.; Chu, J. H.; Betenbaugh, M. J. Assessment of the Coordinated Role of ST3GAL3, ST3GAL4 and ST3GAL6 on the α2,3 Sialylation Linkage of Mammalian Glycoproteins. *Biochem. Biophys. Res. Commun.* **2015**, *463*, 211−215.

(10) Harduin-Lepers, A. Comprehensive Analysis of Sialyltransferases in Vertebrate Genomes. *Glycobiol. Insights* **2010**, *2*, 29−61.

(11) Harduin-Lepers, A.; Mollicone, R.; Delannoy, P.; Oriol, R. The Animal Sialyltransferases and Sialyltransferase-related Genes: A Phylogenetic Approach. *Glycobiology* **2005**, *15*, 805−817.

(12) Veillon, L.; Fakih, C.; Abou-El-Hassan, H.; Kobeissy, F.; Mechref, Y. Glycosylation Changes in Brain Cancer. *ACS Chem. Neurosci.* **2018**, *9*, 51−72.

(13) Büll, C.; Boltje, T. J.; Wassink, M.; de Graaf, A. M. A.; van Delft, F. L.; den Brok, M. H.; Adema, G. J. Targeting Aberrant Sialylation in Cancer Cells Using a Fluorinated Sialic Acid Analog Impairs Adhesion, Migration, and in Vivo Tumor Growth. *Mol. Cancer Ther.* **2013**, *12*, 1935−1946.

(14) Mahal, L. K.; Charter, N. W.; Angata, K.; Fukuda, M.; Koshland, D. E., Jr.; Bertozzi, C. R. A Small-Molecule Modulator of Poly-Alpha 2,8-Sialic Acid Expression on Cultured Neurons and Tumor Cells. *Science* **2001**, *294*, 380−381.

(15) Bernacki, R.; Kim, U. Concomitant Elevations in Serum Sialytransferase Activity and Sialic Acid Content in Rats with Metastasizing Mammary Tumors. *Science* **1977**, *195*, 577−580.

(16) Sotiropoulou, G.; Kono, M.; Anisowicz, A.; Stenman, G.; Tsuji, S.; Sager, R. Identification and Functional Characterization of a Human GalNAc [alpha]2,6-Sialyltransferase with Altered Expression in Breast Cancer. *Mol. Med.* **2002**, *8*, 42−55.
(17) Sasaki, M.; Barber, S.; Ceriani, R. L. Breast Cancer Markers: Comparison Between Sialyltransferase and Human Mammary Epithelial Antigens (HME-Ags) for the Detection of Human Breast Tumors Grafted in Asnnude Mice. *Breast Cancer Res. Treat.* **1985**, *5*, 51−56.
(18) Roncati, L.; Barbolini, G.; Gatti, A. M.; Pusiol, T.; Piscioli, F.; Maiorana, A. The Uncontrolled Sialylation is Related to Chemoresistant Metastatic Breast Cancer. *Pathol. Oncol. Res.* **2016**, *22*, 869−873.
(19) Jones, R. B.; Dorsett, K. A.; Hjelmeland, A. B.; Bellis, S. L. The St6gal-I Sialyltransferase Protects Tumor Cells against Hypoxia by Enhancing Hif-1alpha Signaling. *J. Biol. Chem.* **2018**, *293*, 5659−5667.
(20) Chakraborty, A.; Dorsett, K. A.; Trummell, H. Q.; Yang, E. S.; Oliver, P. G.; Bonner, J. A.; Buchsbaum, D. J.; Bellis, S. L. St6gal-I Sialyltransferase Promotes Chemoresistance in Pancreatic Ductal Adenocarcinoma by Abrogating Gemcitabine-Mediated DNA Damage. *J. Biol. Chem.* **2018**, *293*, 984−994.
(21) Hsieh, C.-C.; Shyr, Y.-M.; Liao, W.-Y.; Chen, T.-H.; Wang, S.-E.; Lu, P.-C.; Lin, P.-Y.; Chen, Y.-B.; Mao, W.-Y.; Han, H.-Y.; Hsiao, M.; Yang, W.-B.; Li, W.-S.; Sher, Y.-P.; Shen, C.-N. Elevation of Beta-Galactoside Alpha2,6-Sialyltransferase 1 in a Fructoseresponsive Manner Promotes Pancreatic Cancer Metastasis. *Oncotarget* **2017**, *8*, 7691−7709.
(22) Szabo, R.; Skropeta, D. Advancement of Sialyltransferase Inhibitors: Therapeutic Challenges and Opportunities. *Med. Res. Rev.* **2017**, *37*, 219−270.
(23) Pérez-Garay, M.; Arteta, B.; Llop, E.; Cobler, L.; Pagès, L.; Ortiz, R.; Ferri, M. J.; de Bolós, C.; Figueras, J.; de Llorens, R.; Vidal-Vanaclocha, F.; Peracaula, R. Alpha2,3-Sialyltransferase St3gal Iv Promotes Migration and Metastasis in Pancreatic Adenocarcinoma Cells and Tends to Be Highly Expressed in Pancreatic Adenocarcinoma Tissues. *Int. J. Biochem. Cell Biol.* **2013**, *45*, 1748−1757.
(24) Bos, P. D.; Zhang, X. H.-F.; Nadal, C.; Shu, W.; Gomis, R. R.; Nguyen, D. X.; Minn, A. J.; van de Vijver, M. J.; Gerald, W. L.; Foekens, J. A.; Massagué, J. Genes That Mediate Breast Cancer Metastasis to the Brain. *Nature* **2009**, *459*, 1005−1009.
(25) Crespo, H. J.; Lau, J. T. Y.; Videira, P. A. Dendritic Cells: A Spot on Sialic Acid. *Front. Immunol.* **2013**, *4*, 491.
(26) Abdu-Allah, H. H. M.; Chang, T. T.; Li, W.-S. Synthesis of B- and C-Ring-Modified Lithocholic Acid Analogues as Potential Sialyltransferase Inhibitors. *Steroids* **2016**, *112*, 54−61.
(27) Rillahan, C. D.; Brown, S. J.; Register, A. C.; Rosen, H.; Paulson, J. C. High-Throughput Screening for Inhibitors of Sialyl- and Fucosyltransferases. *Angew. Chem., Int. Ed. Engl.* **2011**, *50*, 12534−12537.
(28) Chang, K.-H.; Lee, L.; Chen, J.; Li, W.-S. Lithocholic Acid Analogues, New and Potent Alpha-2,3-Sialyltransferase Inhibitors. *Chem. Commun.* **2006**, 629−631.
(29) Fu, C.-W.; Chang, K.-H.; Jen, Y. C.; Chang, T. T.; Li, W.-S. Synthesis of Amino Acid-comprising Sialyltransferase Inhibitors and Their Antimetastatic Activities against Human Breast Cancer Cells. *J. Chin. Chem. Soc.* **2016**, *63*, 171−180.
(30) Heise, T.; Pijnenborg, J. F. A.; Büll, C.; van Hilten, N.; Kers-Rebel, E. D.; Balneger, N.; Elferink, H.; Adema, G. J.; Boltje, T. J. Potent Metabolic Sialylation Inhibitors Based on C-5-Modified Fluorinated Sialic Acids. *J. Med. Chem.* **2019**, *62*, 1014−1021.
(31) Guo, J.; Li, W.; Xue, W.; Ye, X.-S. Transition State-Based Sialyltransferase Inhibitors: Mimicking Oxocarbenium Ion by Simple Amide. *J. Med. Chem.* **2017**, *60*, 2135−2141.
(32) Wang, L.; Liu, Y.; Wu, L.; Sun, X.-L. Sialyltransferase Inhibition and Recent Advances. *Biochim. Biophys. Acta* **2016**, *1864*, 143−153.
(33) Li, W.; Niu, Y.; Xiong, D.-C.; Cao, X.; Ye, X.-S. Highly Substituted Cyclopentane-Cmp Conjugates as Potent Sialyltransferase Inhibitors. *J. Med. Chem.* **2015**, *58*, 7972−7990.
(34) Rillahan, C. D.; Antonopoulos, A.; Lefort, C. T.; Sonon, R.; Azadi, P.; Ley, K.; Dell, A.; Haslam, S. M.; Paulson, J. C. Global Metabolic Inhibitors of Sialyl- and Fucosyltransferases Remodel the Glycome. *Nat. Chem. Biol.* **2012**, *8*, 661−668.
(35) Izumi, M.; Wada, K.; Yuasa, H.; Hashimoto, H. Synthesis of Bisubstrate and Donor Analogues of Sialyltransferase and Their Inhibitory Activities. *J. Org. Chem.* **2005**, *70*, 8817−8824.
(36) Hinou, H.; Sun, X.-L.; Ito, Y. Systematic Syntheses and Inhibitory Activities of Bisubstrate-Type Inhibitors of Sialyltransferases. *J. Org. Chem.* **2003**, *68*, 5602−5613.
(37) Schwörer, R.; Schmidt, R. R. Efficient Sialyltransferase Inhibitors Based on Glycosides of N-Acetylglucosamine. *J. Am. Chem. Soc.* **2002**, *124*, 1632−1637.
(38) Schröder, P. N.; Giannis, A. From Substrate to Transition State Analogues: The First Potent Inhibitor of Sialyltransferases. *Angew. Chem., Int. Ed. Engl.* **1999**, *38*, 1379−1380.
(39) Müller, B.; Schaub, C.; Schmidt, R. R. Efficient Sialyltransferase Inhibitors Based on Transition-State Analogues of the Sialyl Donor. *Angew. Chem., Int. Ed. Engl.* **1998**, *37*, 2893−2897.
(40) Moremen, K. W.; Ramiah, A.; Stuart, M.; Steel, J.; Meng, L.; Forouhar, F.; Moniz, H. A.; Gahlay, G.; Gao, Z.; Chapla, D.; Wang, S.; Yang, J.-Y.; Prabhakar, P. K.; Johnson, R.; Rosa, M. D.; Geisler, C.; Nairn, A. V.; Seetharaman, J.; Wu, S.-C.; Tong, L.; Gilbert, H. J.; LaBaer, J.; Jarvis, D. L. Expression System for Structural and Functional Studies of Human Glycosylation Enzymes. *Nat. Chem. Biol.* **2018**, *14*, 156−162.
(41) Baek, M. K.; Park, J. S.; Park, J. H.; Kim, M. H.; Kim, H. D.; Bae, W. K.; Chung, I. J.; Shin, B. A.; Jung, Y. D. Lithocholic Acid Upregulates uPAR and Cell Invasiveness via MAPK and AP-1 Signaling in Colon Cancer Cells. *Cancer Lett.* **2010**, *290*, 123−128.
(42) Su, M.-L.; Chang, T.-M.; Chiang, C.-H.; Chang, H.-C.; Hou, M.-F.; Li, W.-S.; Hung, W.-C. Inhibition of Chemokine (C-C Motif) Receptor 7 Sialylation Suppresses Ccl19-Stimulated Proliferation, Invasion and Anti-Anoikis. *PLoS One* **2014**, *9*, No. e98823.
(43) Chiang, C. H.; Wang, C. H.; Chang, H. C.; More, S. V.; Li, W. S.; Hung, W. C. A Novel Sialyltransferase Inhibitor Al10 Suppresses Invasion and Metastasis of Lung Cancer Cells by Inhibiting Integrin-Mediated Signaling. *J. Cell. Physiol.* **2010**, *223*, 492−499.
(44) Chen, J.-Y.; Tang, Y.-A.; Huang, S.-M.; Juan, H.-F.; Wu, L.-W.; Sun, Y.-C.; Wang, S.-C.; Wu, K.-W.; Balraj, G.; Chang, T.-T.; Li, W.-S.; Cheng, H.-C.; Wang, Y.-C. A Novel Sialyltransferase Inhibitor Suppresses Fak/Paxillin Signaling and Cancer Angiogenesis and Metastasis Pathways. *Cancer Res.* **2011**, *71*, 473−483.
(45) Isaji, T.; Im, S.; Kameyama, A.; Wang, Y.; Fukuda, T.; Gu, J. A Complex between Phosphatidylinositol 4-Kinase Iialpha and Integrin Alpha3beta1 Is Required for N-Glycan Sialylation in Cancer Cells. *J. Biol. Chem.* **2019**, *294*, 4425−4436.
(46) Ma, H.; Zhou, H.; Song, X.; Shi, S.; Zhang, J.; Jia, L. Modification of Sialylation Is Associated with Multidrug Resistance in Human Acute Myeloid Leukemia. *Oncogene* **2015**, *34*, 726−740.
(47) Almaraz, R. T.; Tian, Y.; Bhattarcharya, R.; Tan, E.; Chen, S.-H.; Dallas, M. R.; Chen, L.; Zhang, Z.; Zhang, H.; Konstantopoulos, K.; Yarema, K. J. Metabolic Flux Increases Glycoprotein Sialylation: Implications for Cell Adhesion and Cancer Metastasis. Mol. *Mol. Cell. Proteomics* **2012**, *11*, M112.017558.
(48) Yamamoto, H.; Oviedo, A.; Sweeley, C.; Saito, T.; Moskal, J. R. Alpha2,6-Sialylation of Cell-Surface N-Glycans Inhibits Glioma Formation in Vivo. *Cancer Res.* **2001**, *61*, 6822−6829.
(49) Winkler, F.; Herz, K.; Rieck, S.; Kimura, K.; Hu, T.; Röll, W.; Hesse, M.; Fleischmann, B. K.; Wenzel, D. Pecam/Egfp Transgenic Mice for Monitoring of Angiogenesis in Health and Disease. *Sci. Rep.* **2018**, *8*, 17582.
(50) DeLisser, H. M.; Christofidou-Solomidou, M.; Strieter, R. M.; Burdick, M. D.; Robinson, C. S.; Wexler, R. S.; Kerr, J. S.; Garlanda, C.; Merwin, J. R.; Madri, J. A.; Albelda, S. M. Involvement of Endothelial Pecam-1/Cd31 in Angiogenesis. *Am. J. Pathol.* **1997**, *151*, 671−677.
(51) Saha, M.; Chakraborty, C.; Arun, I.; Ahmed, R.; Chatterjee, S. An Advanced Deep Learning Approach for Ki-67 Stained Hotspot

Detection and Proliferation Rate Scoring for Prognostic Evaluation of Breast Cancer. *Sci. Rep.* **2017**, *7*, 3213.
(52) Tan, P.-H.; Bay, B.-H.; Yip, G.; Selvarajan, S.; Tan, P.; Wu, J.; Lee, C.-H.; Li, K.-B. Immunohistochemical Detection of Ki67 in Breast Cancer Correlates with Transcriptional Regulation of Genes Related to Apoptosis and Cell Death. *Mod. Pathol.* **2005**, *18*, 374−381.
(53) Sun, Z.; Costell, M.; Fässler, R. Integrin Activation by Talin, Kindlin and Mechanical Forces. *Nat. Cell Biol.* **2019**, *21*, 25−31.
(54) Tanentzapf, G.; Brown, N. H. An Interaction between Integrin and the Talin Ferm Domain Mediates Integrin Activation but Not Linkage to the Cytoskeleton. *Nat. Cell Biol.* **2006**, *8*, 601−606.
(55) Calderwood, D. A. Talin Controls Integrin Activation. *Biochem. Soc. Trans.* **2004**, *32*, 434−437.
(56) Baade, T.; Paone, C.; Baldrich, A.; Hauck, C. R. Clustering of Integrin Beta Cytoplasmic Domains Triggers Nascent Adhesion Formation and Reveals a Protozoan Origin of the Integrin-Talin Interaction. *Sci. Rep.* **2019**, *9*, 5728.
(57) Wang, J.-h. Pull and Push: Talin Activation for Integrin Signaling. *Cell Res.* **2012**, *22*, 1512−1514. (c) Moser, M.; Legate, K. R.; Zent, R.; Fässler, R. The Tail of Integrins, Talin, and Kindlins. *Science* **2009**, *324*, 895−899.
(58) Nader, G. P. F.; Ezratty, E. J.; Gundersen, G. G. Fak, Talin and Pipkigamma Regulate Endocytosed Integrin Activation to Polarize Focal Adhesion Assembly. *Nat. Cell Biol.* **2016**, *18*, 491−503.
(59) Mitra, S. K.; Hanson, D. A.; Schlaepfer, D. D. Focal Adhesion Kinase: In Command and Control of Cell Motility. *Nat. Rev. Mol. Cell Biol.* **2005**, *6*, 56−68.
(60) Liu, S.; Thomas, S. M.; Woodside, D. G.; Rose, D. M.; Kiosses, W. B.; Pfaff, M.; Ginsberg, M. H. Binding of Paxillin to Alpha4 Integrins Modifies Integrin-Dependent Biological Responses. *Nature* **1999**, *402*, 676−681.
(61) Yamada, T.; Tsuda, M.; Wagatsuma, T.; Fujioka, Y.; Fujioka, M.; Satoh, A. O.; Horiuchi, K.; Nishide, S.; Nanbo, A.; Totsuka, Y.; Haga, H.; Tanaka, S.; Shindoh, M.; Ohba, Y. Receptor Activator of Nf-Kappab Ligand Induces Cell Adhesion and Integrin Alpha2 Expression Via Nf-Kappab in Head and Neck Cancers. *Sci. Rep.* **2016**, *6*, 23545.
(62) Ahmed, K. M.; Zhang, H.; Park, C. C. Nf-Kappab Regulates Radioresistance Mediated by Beta1-Integrin in Three-Dimensional Culture of Breast Cancer Cells. *Cancer Res.* **2013**, *73*, 3737−3748.
(63) Wani, A. A.; Jafarnejad, S. M.; Zhou, J.; Li, G. Integrin-Linked Kinase Regulates Melanoma Angiogenesis by Activating Nf-Kappab/Interleukin-6 Signaling Pathway. *Oncogene* **2011**, *30*, 2778−2788.
(64) Klein, S.; de Fougerolles, A. R.; Khan, L.; Pepe, A.; Green, C. D.; Koteliansky, V.; Giancotti, F. G.; Giancotti, F. G. $\alpha 5\beta 1$ Integrin Activates an NF-κB-Dependent Program of Gene Expression Important for Angiogenesis and Inflammation. *Mol. Cell. Biol.* **2002**, *22*, 5912−5922.
(65) Kansy, M.; Senner, F.; Gubernator, K. Physicochemical High Throughput Screening: Parallel Artificial Membrane Permeation Assay in the Description of Passive Absorption Processes. *J. Med. Chem.* **1998**, *41*, 1007−1010.
(66) Kansy, M.; Kratzat, K.; Parrilla, I.; Senner, F.; Wagner, B. Physicochemical High Throughput Screening (pC-HTS): Determination of Membrane Permeability, Partitioning and Solubility. In *Molecular Modeling and Prediction of Bioactivity*. New York: Kluwer Academic/Plenum Press, 2000; pp 237−243. Proceedings of the 12th European Symposium on Quantitative Structure-Activity Relationships: Molecular Modeling and Prediction of Bioactivity, Copenhagen, Denmark. Aug 23−28, 1998.
(67) Astone, M.; Dankert, E. N.; Alam, S. K.; Hoeppner, L. H. Fishing for Cures: The Allure of Using Zebrafish to Develop Precision Oncology Therapies. *npj Precis. Oncol.* **2017**, *1*, 39.
(68) Doak, B. C.; Over, B.; Giordanetto, F.; Kihlberg, J. Oral Druggable Space Beyond the Rule of 5: Insights from Drugs and Clinical Candidates. *Chem. Biol.* **2014**, *21*, 1115−1142.
(69) Shultz, M. D. Two Decades under the Influence of the Rule of Five and the Changing Properties of Approved Oral Drugs. *J. Med. Chem.* **2019**, *62*, 1701−1714.
(70) Harrus, D.; Harduin-Lepers, A.; Glumoff, T. Unliganded and CMP-Neu5Ac Bound Structures of Human α-2,6-Sialyltransferase ST6Gal I at High Resolution. *J. Struct. Biol.* **2020**, *212*, 107628.
(71) Rao, F. V.; Rich, J. R.; Rakić, B.; Buddai, S.; Schwartz, M. F.; Johnson, K.; Bowe, C.; Wakarchuk, W. W.; Defrees, S.; Withers, S. G.; Strynadka, N. C. J. Structural Insight into Mammalian Sialyltransferases. *Nat. Struct. Mol. Biol.* **2009**, *16*, 1186−1188.

https://dx.doi.org/10.1021/acs.jmedchem.0c01477
J. Med. Chem. 2021, 64, 527−542